East Siberian Arctic background and black carbon polluted aerosols at HMO Tiksi.

O. Popovicheva[1]*, L. Diapouli[4] , A. Makshtas[2] , N. Shonija[3], E. Kireeva[1], D. Saraga[4], T. Uttal[5], and K.Eleftheriadis[4].

[1]Scobeltsyn Institute of Nuclear Physics, Lomonosov Moscow State University, 119991, Moscow, Russia
[2]Arctic Antarctic Research Institute, St.Peterburg, 199397, Russia
[3] Chemical Department, Lomonosov Moscow State University, 119991, Moscow, Russia
[4]N.C.S.R. "Demokritos", Athens, 15310, Greece
[5]National Oceanic and Atmospheric Administration, Boulder, Colorado USA

Abstract.

Assessment of Arctic air pollution is hampered by a lack of aerosol studies in Northern Siberia. Black carbon (BC) observations were carried out at the Hydrometeorological Observatory (HMO) Tiksi, a coast of Laptev sea, from September 2014 to September 2016. Aerosol sampling in seven periods of autumn, winter-spring, and early summer was accompanied by physico-chemical characterization. Monthly BC climatology showed a seasonal variation with highest concentrations from January to March (up to 450 ng/m^3) and lowest ones for June and September (about 20 ng/m^3). Background periods were irregularly changed by episodes of increased BC lasting during a few days. Stagnant weather and stable atmosphere stratification were resulted in accumulation of pollution from regional and local sources, in dependence on the wind direction and air mass transportation. Carbon (OC,EC) fractions, inorganic/organic functionalities, ions, and elements are associated to marine, biogenic, and continental sources. EC demonstrate a strong seasonability, well in accordance with BC, while OC and sulfates in autumn are fairly high, being significantly influenced by local activities. In September low OC, aliphatic, carbonyl, amino, and hydroxyl functionalities characterize background aerosols of biogenic and oceanic activity. The ratio Na^+/Cl^- much higher than in sea-salt aerosols indicates a strong Cl depletion. Increased OC, up to 3.7 μg/m^3, aromatic, carbonyls, and nitrocompounds as well as waste burning markers K^+, Cl^-, and PO_4^{2-} ions confirm the impacts of Tiksi landfill burns as a consistent local source. BC pollution episodes are differentiated through a few times increased EBC and sulfates up to 150 ng/m^3 and 1.6 μg/m^3, respectively, related to gas flaring, industrial and residential emissions transported from Western Siberia, Krasnoyarsk Krai, and Lena river delta while the significant increase of carbonyls, hydroxyl, and aromatic indicate emissions sources from central Yakutia and adjacent

* Correspondence to: O. Popovicheva polga@mics.msu.su

Tiksi urban area. In winter-spring, the Arctic Haze aerosols are characterized by increased concentrations of SO_4^{2-} in comparison with OC, much higher abundance of oxygenated compounds with respect to alkanes of anthropogenic origin. Early in summer high organic mass and rich organic chemistry indicated the high impacts of both natural biogenic emissions, local urban and shipping sources as well as secondary aerosol formation influenced by industrial and fire emissions from low latitude Siberia.

Keywords: aerosol, Russian Arctic, physical-chemical characteristics, black carbon, organic carbon, sulfates, sources of pollution.

1. Introduction.

Arctic atmospheric data are critical to evaluate climate-active species trends and global impacts. Currently, risks and uncertainties regarding climate change have become the focus of intense research efforts. Warming in the Arctic has been accompanied by ice loss, reduction of the surface albedo, changes in the hydrological balance and positive feedbacks leading to further warming. Carbonaceous aerosols have contributed 1.09 ± 0.81 °C to the observed Arctic temperature increase of 1.48 ± 0.28 °C from 1976 to 2007 (Shindell and Faluvegi, 2009). In winter-spring, the combination of intense isentropic transport from mid-latitudes to the Arctic and strong surface-based temperature inversions results in a large increase of tropospheric aerosol concentration known as Arctic Haze (Quinn et al., 2008). The springtime when the sunlight returns is the most critical time for aerosol induced Arctic warming. In contrast to the Arctic Haze period, summer months are much cleaner due to the retreat of the polar front which blocks long-range pollutant transport into the Arctic, although the influence of local sources may become relatively stronger.

Black carbon (BC) is the climate-active fraction of aerosols absorbing sunlight. Originating from local and regional combustion sources together with organic carbon (OC), BC exerts a warming effect that contrasts to cooling effect of scattering sulfates. BC residing in the lowest atmospheric layer impacts aerosol-cloud interactions (Yun et al., 2013) and produces the Arctic warming because of cloud and sea-ice feedback (Flanner, 2013). BC decreases the snow albedo when precipitating out of the atmosphere, absorbing sunlight on the surface and accelerating snowmelt (Quinn et al., 2008). OC could result in either positive or negative feedbacks to global warming (Tomasi et al., 2007), making the understanding of the role of organics in the Arctic atmosphere crucial for quantifying the direct and indirect aerosol effects (Fu et al., 2009). Since climate change is proceeding fastest in the high latitudes (Law and Stohl, 2007), there is an increasing need for better understanding the sources of aerosol pollutants in the Arctic. Organic functional group composition provides important insight on the sources and composition of springtime Arctic haze and the substantial organic matter contributions into season-dependent mass concentrations (Shaw et al., 2010).

Studies of aerosol composition have significantly expanded the knowledge about BC and OC pollution in the Arctic (Chang et al., 2011; Nguyen et al., 2013; Stohl et al., 2007). Source apportionment has relied on a combination of elemental carbon (EC) and OC tracers (Barrett et al., 2015; Chang et al., 2011; von Schneidemesser et al., 2009). Transport, industry, gas flaring, and residential emissions are assumed to be responsible for anthropogenic BC and OC in the Arctic (Stohl et al., 2013; Wang et al., 2011). The isotope-constrained source apportionment pinpointed that biomass burning was dominant during low BC concentration seasons in summer whereas fossil sources impacted during the Arctic haze seasons (Winiger et al., 2017). However, the sources and chemical composition of arctic aerosols are still poorly represented in models. Even the most recent emission inventory has an estimated range of total BC emissions that spans one order of magnitude (Huang et al., 2015).

Observations of high levels of the Arctic pollution due to BC transport from Eurasian Russia has been recorded at several Arctic stations including Barrow (Alaska), Alert (Canada), Summit (Greenland), and Zeppelin, Ny-Ålesund (Svalbard) (Sharma et al., 2013; Sharma et al., 2004; Treffeisen et al., 2007; von Schneidemesser et al., 2009). BC monthly climatology has been compared, documenting the marked maxima in winter and minima in summer and early autumn (Stone et al., 2014) while Siberian arctic atmospheric aerosol data are remaining to be very limited. Currently, a few BC measurements are available in East Siberian Arctic; mostly campaigns that measured BC in the Arctic sea (Popovicheva et al., 2017a; Sakerin et al., 2015; Stohl et al., 2013) and remote sensing measurements of aerosol optical depth on the drifting station "North Pole" (Stock et al., 2012).

Hydrometeorological Observatory (HMO) Tiksi (71.36N; 128.53E), located on the coast of Laptev sea in Northern Siberia takes place closer to the BC source regions of high-latitude Eurasia than other arctic stations (Hirdman et al., 2010). It has been previously a site for short-term BC and aerosol composition (element, OC, EC) measurement (Makarov et al., 2007; Rahn et al., 1997; Sakerin et al., 2012). Continuous observations of equivalent black carbon (EBC) with an aethalometer were started at the HMO Tiksi in 2009 (Eckhardt et al., 2015) followed by aerosol number density and size distribution measurements (Asmi et al., 2016). In 2009-2010 years the annual mean EBC concentration was found 2.5 times higher than for other arctic stations due to the possible influence of regional and local sources**.** However, ongoing Arctic aerosol studies almost present the averaged data remaining the consideration of the episodes of high BC to be highly limited. Therefore, the observations based on comprehensive characterization of aerosol composition should be performed to increase the ability of identification of episodes related with potential pollution sources in the Arctic atmosphere.

In this paper is devoted to BC observations coupled with comprehensive aerosol characterization performed at the HMO Tiksi during seven sampling periods of 2-years study, namely in September 2014, 2015 and 2016, November 2014, March 2015, May-June 2015, and June 2016. Real-time measurements of aerosol light absorption quantify the periods of the background replaced by episodes of the increased EBC. Analyses of wind and BC pollution roses combined with long-range transport identify the episodes of

pollution source impacts either from lower latitudes or/and local emissions from the adjacent urban Tiksi area. We firstly present the characteristics of aerosols such as carbon fractions (OC,EC), inorganic and organic functionalities of chemical compounds, ion components, and elements which characterize the season background and pollution episodes providing the complementary insight on source-influenced and season-dependent composition of East Siberian Arctic aerosols.

2. Experimental.

2.1. Sampling.

The International HMO Tiksi was established through an cooperation during the International Polar Year (Uttal et al., 2013) and included the construction of the weather station, Clean Air Faciity (CAF) for aerosol and gas sampling, and meteorological flux tower. The aerosol measurements described here were taken at the CAF that is located approximately 1 km north from the weather station Polyrka, 500 m from the Laptev sea coast, and near 5 km from the Tiksi settlement, from which it is separated by a hill (Fig.1). The 20 meter Tiksi meteorological flux tower is located around 300 meter from the CAF; multiple levels are instrumented for the measurement of air temperature, relative humidity, and wind speeds allowing calculations of profiles in the near surface boundary layer. The basic meteorological parameters, such as wind speed, wind direction, temperature, relative humidity, and pressure were obtained every 3 hours at weather station Polyrka. All local values were converted to UTC time.

The area of the Tiksi settlement is separated on two parts which are located in the direction north and north-east from the CAF (Fig.1). Aeroport Tiksi takes place in the northern part of a city. There are a few urban emissions sources in the Tiksi settlement such as a power plan using crude oil, the heating stations, and intensive tranport. Tiksi settlement is located at the Arctic Ocean coast of the remote Far East and serves as one of the biggest ports for accessing the Laptev Sea, therefore shipping emission can be another responsible BC source. At certain times the plume from Tiksi may disturb the background aerosol and gaseous measurements at the CAF with local pollution, which we can identify by screening the data obtained when the wind arrives in the directions of 300-360 and 0-50 degrees, as shown in Fig.1. Therefore, the sector of the north-west – north – north-est wind is assigned to “Local Pollution Influenced (LPI)”. In (Asmi et al., 2016) the wind direction was expressed as percentages from the 45–150 degree sector (marine sector) and from the 150–315 sector (continental sector), leaving out the sector defined as polluted.

A seven wavelengh aethalometer (AE-31, Magee Scientific) is operated at the CAF measuring aerosol optical properties by detecting the attenuation of light transmitted through particles that are accumulated on a quartz fiber filter. 5-min averages of BC data from the aethalometer were acquired continuously. Equaivalent black carbon (EBC) was caclulated at 880 nm using the instrument specific mass absorption coefficient as 16.6 $m^2 g^{-1}$. Only during very clean period of sampling in May-June 2015 the EBC data collected at 660 nm was evaluated. Three short duration extreme EBC values appeared on 24.09, 30.09, and 24.11 of 2014 were removed from database, they appeared to be a result of an instrument malfuction.

An aerosol sampling system was installed at the CAF in September of 2014 to provide aerosol samples complementary to the real-time BC monitoring. A total suspended particle (TSP) inlet was installed approximately 1.5 m above the CAF roof and 5 m above the ground. TSP inlet has an antifreeze system to prevent water directly entering into the inlet and ice blocking the system. Aerosols were sampled at an air flow of ~ 45 l/min and collected into a temperature controlled room. The flow rate was obtained using standard barometric pressure and temperature on the basis of in situ meteorological conditions presented in Table 1.

TSP particles were collected on 47 mm quartz fiber (Pallflex) and teflon (Zeflour) filters for subsequent analyses in a laboratory. Low concentration of ambient aerosols necessitates sampling times from one day in November up to three days in September to allow the loading exceeds the detection limit for relevant aerosol chemistry analyses. Custom-made two-stage cascade impactor with the aerodynamic cut-offs of 5.5 and 0.33 μm for first and second stage, respectively, was utilized to collect particles on metal substrate (Ti foil) installed on the second stage. Collection duration (typically lasted 30-50 min) was adjusted to avoid overloading.

Due to harsh winter conditions and the remoteness of the CAF site only limited sampling periods could be available. It was performed in September and November of 2014, in March, May-June, and September 2015, and in June and September 2016. The sampling periods, times, and average ambient conditions are presented in Table 1. Stability of the atmospheric surface layer during sampling periods is estimated by the stratification parameter Z/L at the altutude Z=10 m where L is the Monin-Obuchov's length in the semi-empirical theory of the turbulent atmosphere (Makshtas, 2012). For estimations of the stratification parameter the hourly averaged profile data are taken from the meteorological flux tower.

Backward trajectories are generated to visualize the atmospheric transport and evaluate the general flow patterns of air masses during sampling days. NOAA HYbrid Single-Particle Lagrangian Integrated Trajectory (HYSPLIT) model of the Air Resources Laboratory (ARL) (Stein et al., 2015) is used. The potential source areas are investigated using 7-day back trajectories for air masses arriving each 6 hours to the HMO Tiksi at 250, 500 and 1000 m heights above sea level (A.S.L.). Forward trajectories from Kamchatka are generated to emphases the possible plume transportation from volcano eruptions. Fire maps covering the studied period are obtained by the Fire Information for Resource Management System (FIRMS), operated by the NASA/GSFC Earth Science Data Information System (ESDIS). Daily maps are related to the computed trajectories, providing a clear picture of the geographical location of fires.

2.2. Methods and analyses.

Table 2 present the aerosol techniques used for sample analyses. Organic (OC) and elemental carbon (EC) were measured by thermo-optical transmittance (TOT) instrument (Lab OC-EC Aerosol Analyzer, Sunset Laboratory, Inc.). Quartz filter samples were heated first up to 650°C in He and then in an mixture of 2% O_2 in He until 850°C, using controlled heating ramps of the EUSAAR_2 thermal protocol (Cavalli et al.,

2010). OC evolved in the inert atmosphere while EC was oxidized in the He-O_2 atmosphere. Charring correction was applied by monitoring the sample transmittance throughout the heating process. 0.2 μg C cm^{-2} was the analytical limit of detection (LOD) for the TOT instrument. This protocol has been initially developed for regional background sites. Before sampling, the quartz fiber filters were pre-treated at 500°C for 6 hours to remove possible OC contaminations. Lab and field blanks were prepared and run following the same procedures as adopted for the samples.

Water soluble ion components were measured by capillary electrophoresis using the Capel 103 system (Lumex) with the UF detection, as described elsewhere (Popovicheva et al., 2016a). One quarter of the sample was extracted in 5 ml of distillated water by ultrasonic agitation for 45 min and then the extract was filtered. Inorganic anions and cations were measured in aqueous extracts with the relative standard deviation of (Popovicheva et al., 2016a)10%, Table 2. A mixture of benzimidazole, tartaric acid, and 18-crown-6-ether was used as an electrolyte in cation measurements. Anions were analyzed in the chromate buffer prepared from chromium oxide (VI), diethanolamine, and cetyltrimethylammonium hydroxide solution. The LOD for ion concentrations was in the range of 0.1-0.5 mg/l depending on the ion type. A few extracts were analyzed by both capillary electrophoresis and ion chromatography as described in (Zhang et al., 2013). Data intercomparison showed the low difference for Mg^{2+}, NO_3^-, K^+, and SO_4^{2-}, near 3-7%. However, the difference for Cl^-, Na^+, and Ca^{2+}, and NH_4^+ approached 11-28%, and 33%, and 47%, respectively, due to high pollution of blank filters with respect to these ions observed in the test measurements before sampling. Mass concentrations of non-sea salt (nss) SO_4^{2-} and (nss) K^+ ions were derived by subtracting the sea salt contribution estimated from Na^+ mass concentration and sea water weight ratio taken for sulfates and potassium as $SO_4^{2-}/Na^+=0.252$ and $K^+/Na^+=0.0353$, respectively.

The functionalities of various inorganic and organic compounds in the entire aerosol composition was analyzed by Fourier Transform Infrared (FTIR) spectroscopy, as described elsewhere (Popovicheva et al., 2017b). Shimadzu IRPrestige-21 spectrometer was used in the diffuse reflectance mode. Spectra were measured at 4 cm^{-1} resolutions for a wavenumber range from 4000 to 500 cm^{-1}. In the case of samples collected on quartz filters, spectral bands with wave numbers in the range below to 1400 cm^{-1} were not considered because of the strong absorption of filter material in this range. The spectra were obtained from five different spots to address the possible inhomogeneity of the sample loading. If four from five spectra demonstrate the same absorption features, we consider these bands as the representative spectrum for the entire sample. IR Solution software was applied to subtract the FTIR spectrum of blank substrates, to correct the baseline absorbance as well as to perform the Kubelka-Munk (K-M) conversion into a quasi-quantitative spectrum which correlates with the sample concentration. Because of the possible overlapping of vibration bands the functionality identification was accomplished through the use of the Shimadzu FTIR database and a set of authentic chemical standards measured in the same FTIR setup, that is the approach taken in previous studies (Coury and Dillner, 2009; Maria et al., 2002).

Teflon filter samples were analysed by an ED-XRF system (E5 Panalytical). The instrument is calibrated for aerosol filters by means of Micro Matter thin standards (evaporated on Mylar 6.3 μm film), as well as NIST CRMs 2584 and 2583 dust deposited on PTFE filters for 35 elements. Analytical uncertainty ranges from 0.3 to 10% and detection limit from 1 to 30 ng/cm^2 depending on element.

3. Results and discussion.

3.1. BC climatology.

Meteorological variables (i.e., temperature, pressure, radiation, winds, and air mass origin) in the Tiksi region have a strong seasonal cycle (Asmi et al., 2016). Median temperatures stay above 0^0C for four months each year between June and September. This period is characterized by the highest-frequency occurrence of marine air masses and the most stable wind speeds with median values ranging from 3 to 5 m/s. In October solar insolation is decreased, resulting in a temperature shift to below 0^0C until January–February, after which the increasing solar radiation resulted in an increasing temperature. The cold month winds were primarily continental. October through December, very high wind speeds occurred with half hour averages of up to 20 m/s indicating stormy weather conditions. January through March is the calmest period of the year, with median wind speeds between 1 and 3 m/s. A shift in weather conditions occurs in April–May with increasing temperatures and stronger winds and the onset of more frequent marine air flow.

In 2009-2010 years high EBC concentrations, more than 100 ng/m^3, and low ones about 20 ng/m^3 were observed in winter - spring and summer - early autumn, respectively (Eckhardt et al., 2015). Monthly BC climatology analyzed during the period of our study shows the similar trend (Fig.2). From September 2014 to September 2016 a distinct EBC seasonal variation with highest concentrations from January to March (230-130 ng/m^3) and lowest from June to August (about 20 ng/m^3) is observed. On average, concentrations in summer were about 10 times lower than those in winter. During winter months the mean EBC concentrations approached higher values, 230±86 and 300±140 ng/m^3 in 2015 and 2016 years, respectively, in comparison with 100±65 ng/m^3 observed at the Alert station, as the maximum found in comparison with observations on other stations. This finding confirms the conclusion of (Eckhardt et al., 2015) and (Winiger et al., 2017) that the HMO Tiksi is the station mostly influenced by emissions from high-latitude Siberia.

3.1.1. Autumn

In order to estimate how frequent EBC concentrations were varied from background to pollution level in summer-autumn, daily BC climatology is analyzed from August to October of 2014, 2015, and 2016. Background air conditions are defined as a state without any detectable influence of local or regional pollution (Eleftheriadis et al., 2004; Mikhailov et al., 2017); in this study we relate the arctic background to the lowest light absorption. Figure 3a shows the summer-autumn periods of the lowest EBC (less than 30 ng/m^3) irregularly changed by episodes of increased EBC up to 230 ng/m^3 lasting typically during 1-3 days.

In **September 2014** the sampling period is characterized by EBC daily mean concentrations around 20 ng/m^3 during the background episode following by the incursion of pollution with the EBC approached

160 ng/m^3 (Fig.4). Analyses of both the wind (Fig.S1) and BC pollution (Fig.5) roses shows that the south-west wind occurred with the greatest frequency which brought the high EBC level while the neutral stratification of the atmospheric boundary layer with near the HMO Tiksi was indicated by Z/L near zero (Fig. S2). Thus, we can hardly assume the impact of local sources from the Tiksi direction on increased EBC level.

Back-trajectory analysis in conjunction with a map has revealed two distinct origins of air masses: until 26.09 they arrived from central Siberian Plateau, then they changed the direction to the Arctic Ocean and passed the coastal areas before arriving to the Tiksi region (Fig.6a). During the episode of increased EBC on 01.10 the transport of air masses was from northern Siberia, from Yamal-Nenetz and Khanty-Mansisky regions where the biggest gas flaring, industrial and residential emission sources in Western Siberia take place, as evaluated in (Huang et al., 2015) and (Winiger et al., 2017). Remarkably that air masses transported from those regions were descended from high altitudes, around 4 km A.S.L. (Fig.6a) where the highest concentrations in the vertical EBC profiles were observed (Brock et al., 2011; Eckhardt et al., 2015). That indicates the impact of different atmosphere layers mixing onto eastern Siberian pollution.

The newly reconstructed inventory of (Huang et al., 2015) indicates a large residential and industrial region near Norilsk in Krasnoyarsk Krai as well as distributed transport emissions including intensive shipping in Lena river delta. We should note that high-latitude Eurasia with the metal smelting complexes were emphasized to be the dominant BC and sulfates source region for other arctic stations such as Ny-Ålesund, Alert and Barrow (Hirdman et al., 2010). Since the days of BC pollution were characterized by the wind speed around 5 m/s followed by stagnant weather we associate this episode to long-range transport (LRT) of polluted mass (Fig.4) which could result to the accumulation of the pollution in the atmosphere near the HMO Tiksi.

In **September 2015** the sampling captured a period of high EBC concentrations in its declining phase when EBC approached 250 ng/m^3 (Fig.3). Before this maximum EBC showed slightly increased level of 50 ng/m^3 (Fig.4), then on 08.09 air masses arrived to Tiksi region from central Yakutia (Fig.6a) where the transport and industrial emissions are quite abundant (Huang et al., 2015). At the end of the sampling period, on 10.09, EBC dropped to the background, and the origin of back trajectories was changed to the north-western region of Krasnoyarsk Krai with low residential and industrial BC emissions.

In distinguishing from the sampling episode in September 2014, the calm (~1 m/s) wind from north was dominated (Fig.S1). During BC pollution episode the north-east wind with speed ~5 m/s was changed to calm from north, the direction from the LPI sector, well coincided with the significant increase of the stratification parameter Z/L up to 8 (Fig.S2). Such combination of meteorological characteristics indicates the favorable conditions for accumulating of contaminations in the atmosphere relating to the strong stratification of the boundary layer in the case of stagnant weather. At that time EBC concentration approached the maximum indicating the largest impact from the local urban emissions (Fig.4).

Sampling in **September 2016** was occurred at the beginning of the high EBC period (Fig.3), from the background level when air masses on 11.09 were originated in the ocean (Fig.6a). Later, LRT from central Yakutia led to increase of EBC exhibited by three maximum (with a period of around one a day) of 172, 130, and 160 ng/m^3 (Fig.4). The calm wind from north was dominated with the frequency about 13% (Fig.S1), however this sampling period was characterized by a high variability of the wind direction including western and north-eastern. The first and third maximum of EBC was observed when the wind was blowing from west, on 13.09 are masses arrived from central Siberia (Fig.6a) while the north-east wind brought the second EBC maximum impacted by local urban emissions from the LPI sector (Fig.4). When EBC approached the second maximum the wind changed down to calm, leading to the coincided increase of the stratification parameter Z/L, up to 12, and indicating the stable atmosphere (Fig.S2) relating to the accumulation of the pollution. Thus, we assign these episodes of BC pollution to complex LRT and local source impacts.

3.1.2. Winter-spring-early summer.

November and March are winter months on the Laptev sea coast, continental winds are prevalent (>50% of the time) opening the gates for low altitude transport of Eurasian pollution into the Arctic (Asmi et al., 2016). The ocean was frozen and deep snow cover was consistent near the HMO Tiksi. Low wind speeds and cold temperatures during winter period suggest a shallow boundary layer in which pollution could be accumulated. At various Arctic locations such as Ny-Alesund, Alert, and Barrow atmospheric aerosols in winter-spring are disturbed by the well-known Arctic Haze, an Arctic pollution phenomenon (Hirdman et al., 2010). The climatology of atmospheric transport from surrounding regions showed that these stations are highly sensitive to emissions from high-latitude Eurasia (Eleftheriadis et al., 2009; Sharma et al., 2004).

In winter, the daily BC climatology is analyzed from November 2014 to January 2015 (Fig.3). As well as in autumn, the periods of low EBC were irregularly changed by episodes of increased EBC but the lowest level of aerosol light absorption related to the background was higher, around 100 ng/m^3, and EBC maximum was approached on average to 300 ng/m^3. During sampling episode in **November 2014** the south-west direction of the wind with the speed more 1 m/s was dominant but the calm wind (<1 m/s) was occurred preferably from the north, from the LPI sector, with the highest frequency around 36% (Fig.S1). Due to stagnate weather high EBC was accumulated, in accordance with stable stratified atmosphere characterized by Z/L~12 (Fig.S2), that is well in correlation with observations of high atmospheric stability in arctic winter (Quinn et al., 2008). During the whole sampling period air masses arrived to the HMO Tiksi from center of Siberian Plateau (Fig.6b). BC pollution episode with highest EBC up to 450 ng/m^3 was observed on 25.11 when the wind blew from south-west and air masses arrived from Yakutia (Fig.6b).

As sunlight returns to the Arctic in spring, the atmospheric stability is reduced and aerosols can be lost with deposition. Aerosol mass transported from lower latitudes is less frequent compared to winter (Stohl, 2006). Figure 3 shows the daily BC climatology from March to June 2015. The sampling period in **March 2015** is characterized by even higher background, around 120 ng/m^3, than in winter (Fig.4). Analyses

of both the wind (Fig.S1) and BC pollution (Fig.5) roses shows that the calm (<2 m/s) north wind occurred with the greatest frequency (28%) which brought the high EBC level (>180 ng/m^3) observed almost during the whole sampling period with frequency around 30%. And we should note the prominent impact of calm wind from north-east, also from the LPI sector. Such a case happen is distinguishably different from other winter and autumn periods although the stable stratification was quite prominent (Fig.S2). The episode of local pollution with highest EBC up to 300 ng/m^3 was observed on 20.03 when the wind blew from the LPI sector. Air mass transport from lower latitudes was prevalent at that time (Fig.6b) demonstrating that the dominant EBC source region was Yakutia, north and central Siberia.

In transition period of late spring – early summer the Arctic front has retreated furthest north and the lower Arctic atmosphere is nearly closed off from continental influence (Sharma et al., 2004). This phenomenon is associated with a general trend of EBC concentration decrease from March to June (Fig.3) and more frequent transport of air masses from the Arctic and Pacific Ocean. In the beginning of the sampling period in **May-June 2015** the EBC background was near the detection limit showing extremely clean atmosphere (Fig.4), at that time air masses arrived from Bereng sea along the coast of East Siberian sea. But later, they changed the transport, and on 03.07 they passed through Eastern Siberia covered by numerous fires (Fig.6b) that could lead to increased EBC measured at the HMO Tiksi. Fires in Russia typically occur during the springtime snowmelt that can more than double the high seasonal Arctic atmospheric background thus impacting climate-relevant species, including black carbon and organic aerosols (Warneke et al., 2010). Analyzes of the BC pollution rose indicates the whole range of EBC concentrations in this sampling period related to the wind direction from the LPI sector, with the frequency of 55% (Fig.4), including the BC pollution episode of 130 ng/m^3, happen in almost neutral atmosphere (Fig.S2).

BC climatology with frequently repeated episodes of increased EBC was observed in one year, during the sampling period in **June 2016** (Fig.4). The wind was varied between west and north-east with the highest frequency from the LPI sector, around 30% (Fig. 5) while EBC was changed almost each day, quite well relating to the atmosphere stratification (Fig.S2). Air masses arrived from the arctic region on days of increased EBC; on 07.06 of highest EBC they transported through the Eurasian coast from western Siberia and Yamal peninsula where numerous fires were observed (Fig.6b). At that time the descent of air masses from 3.5 km altitude was observed. It is worth noting that chemical compounds released by large fires may be injected into the atmosphere up to altitudes of several kilometers (Trentmann et al., 2006). The BC pollution episode of the highest EBC, up to 170 ng/m^3, was happened when north-east wind (50-100^0) was blowing from the Tiksi area where the marine habour takes place (Fig.1) therefore we should also emphases the potential shipping emission impact.

BC, being a short-living climate forcer, may serve as a tracer of the arctic pollution, allowing a link to climate response, if aerosol characteristics relating to combustion emission sources are defined. In the following sections, aerosol physico-chemical characteristics observed in sampling periods will be described, and the features of natural background and specific ones for the BC pollution episodes will be identified.

3.2. Aerosol chemistry.

Black carbon in combustion aerosols has microcrystalline graphitic form of elemental carbon (EC) (Baumgardner et al., 2012). The comparison of EC obtained by thermal analysis with EBC from optical absorption measurements has identified the season variation of aerosol chemistry (Sharma et al., 2004) and quantified the site specific mass absorption coefficient (Stone et al., 2014). Low EBC ~ 8 ng/m^3 were obtained in June - September at the Alert station (Sharma et al., 2004), well in the range of the arctic background. In (Barrett et al., 2015) six week-long winter samples collected at the Barrow station showed the EBC ranging from 40 to 100 ng/m^3, from December to February, respectively. Aerosol samples collected during 21-84 days of two years observations at the RAS Polar Geocosmophysical (PGC) Observatory (which takes place 10 km south from HMO Tiksi) demonstrated a strong seasonability of averaged EC concentrations, ranged from 8 to 302 ng/m^3 from July to February (Winiger et al., 2017).

Figure 7a shows EC concentrations measured at the HMO Tiksi during autumn and winter-spring from September 2014 to September 2016. Samples were collected during 1-3 days that well fits to time duration of EBC variations, as shown by BC climatology study above. Moreover, EBC concentrations were varying from 8 ng/m^3 in September to 198 ng/m^3 in November, well demonstrating the season trend typical for the arctic aerosol concentrations marked by maxima in the winter months and minima in summer (Stone et al., 2014). EBC averaged over the time of the corresponding sample collection is shown in Table 1, the averaged BC/EC ratio is found equal to 1.33. This ratio is well within an expected difference derived from two methods of BC and EC measurements (Baumgardner et al., 2012). EC values during the whole periods of our study well correlate with EBC, with a high correlation coefficient R^2= 0.78 (Fig.S3) that shows the high quality of performed chemical analyses and real-time measurements.

Organic carbon (OC) compose a significant fraction of total submicron aerosol mass in the Arctic (Chang et al., 2011). OC tends to be elevated owing biogenic emissions and secondary aerosol formation from biogenic volatile organic compounds, wind-induced bubbles bursting from the sea surface (Frossard et al., 2014), fossil fuel combustion (Barrett et al., 2015) as well as biomass burning (agricultural and wildfires) (Stohl et al., 2007; Warneke et al., 2010). At the HMO Tiksi OC concentrations in winter-spring sampling periods were varying from 0.6 µg/m^3 in May to 2.3 µg/m^3 in November (Fig.7), that may relate to the general season variation of arctic aerosols. However, OC concentrations in September are found to be fairly high, up to 3.7 µg/m^3, to follow well the decreasing tendency in summer-autumn in comparison with winter. Such observation indicates that out sampling duration well followed the episodes of local OC pollutions which could bring the extensive amount of organic compounds to arctic aerosols in early autumn.

The high OC/EC ratio in aerosol composition characterizes the natural background due to high OC in comparison with negligible EC. While in the urban environment OC is comparable to EC dominated by traffic and fossil fuel combustion (Samara et al., 2014). At the PGC Observatory during two years of observations the highest OC/EC, up to 30, was observed in summer and autumn, until the middle of October, and then it decreased down 5 in winter and spring (Winiger et al., 2017). Qualitatively the similar trend is

observed in our study (Table 1): the biggest OC/EC in September periods and lowest in November and March.

Long-term surface measurements indicate that arctic aerosols consist mainly of sulfates and to a lesser extent of organics, ammonium, nitrates, and BC (Quinn et al., 2007). The main contribution of biological activity of ocean and Arctic pack ice is resulting in a significant production of dimethyl sulfide CH_3SCH_3 which oxidize and form various sulfur-containing products such as sulfuric acid H_2SO_4 and methyl sulfonic acid CH_3SO_3H (Yin et al., 1990). High sulfate concentration can relate to regional sources of secondary sulfate aerosol formation during periods of air mass transportation from continent (Eckhardt et al., 2015). A strong seasonal variation correlation found between BC and sulfate concentrations (Hirdman et al., 2010) indicates that they both have similar anthropogenic sources and mainly located in high-latitude Arctic (Eleftheriadis et al., 2009; Sharma et al., 2013). Na^+, Cl^-, K+, and Mg^{2+} are the major ions in the sea-salt aerosols which are ubiquitous in the marine boundary layer and significantly impact the particle concentrations in coastal regions (Li and Winchester, 1989). Ammonium NH_4^+ is mainly produced by soil and emission from vegetation and ocean, its common form can be $(NH_4)_2SO_4$ and NH_4Cl. As well as sulfates, ammonium is influenced by regional sources of secondary aerosol formation and transport.

Figure 7b shows the mass concentrations of inorganic SO_4^{2-}, Na^+, Cl^-, NH_4^+, K^+, Mg^{2+}, NO_3^-, PO_4^{3-}, and F^- ions in water-soluble fraction of aerosols during the sampling periods at the HMO Tiksi. Total ion mass concentration well demonstrates the season variation similar to one for SO_4^{2-}. The season cycle of sulfates shows a clear maximum during the Arctic Haze and a minimum in summer/early autumn but also with fairly high values in September similar to OC. In chemical models which assume the similar sources of origin, their internal mixture, and similar removal process the high season correlation for EBC and SO_4^{2-} concentrations were found (Eckhardt et al., 2015). Our data show a small correlation between EC and sulfates with $R^2 = 0.3$ that means that ocean sulfate productions are more prominent if compare with combustion sources or sulfates are produced by local source which not always relate with high-temperature combustion. OC concentrations in winter are found at less concentrations than SO_4^{2-} but higher in autumn and summer that additionally indicate impact of local pollutions from OC emissions as well as from fires which could bring the extensive amount of organic compounds to arctic aerosols in early autumn.

3.2.1. Autumn.

At the beginning of the background period **in September 2014** (Fig 4), when the tundra was snow-free and the wind was blowing from south-west, OC was originated from biogenic and marine activity with concentration ~ 600 ng/m^3. The organic functional group composition provides an important insight on the sources and composition. Analyses of absorption bands shows aliphatic C-C-H (2931-2855 cm^{-1}), carbonyl C=O (1731 cm^{-1}), amino N-H (3247 cm^{-1}), and hydroxyl C-OH (3547 cm^{-1}) groups in alkanes, esters/lactones, aminocompounds, alcohols/phenols, respectively (Fig.8a). Carbonyl and amino functionalities are particularly relevant to biogenic aerosols being characteristic of primary and secondary organic aerosol formed by oxidation of biogenic volatile organic compounds (BVOC) (Hawkins and Russell,

2010). Impact of BVOC emissions from Siberian boreal regions on the aerosol number distribution at the HMO Tiksi was shown in (Asmi et al., 2016). (Russell et al., 2010) has assumed that hydroxyl functional groups with a broad absorbance between 3200 and 3500 cm^{-1} of carbohydrate-like compounds, including saccharides, are associated with ocean-derived particles emitted by bubble bursting during wave breaking. Bands of CO_3^{2-} in carbonates peaked at 871 cm^{-1} and ammonium NH_4^+ (3247 cm^{-1}) characterize the absorption of inorganic natural aerosol.

At that time the concentration of Na^+ and Cl^- ions is found ~300 and 30 ng/m^3, respectively. Remarkably that the ratio Na^+/Cl^- is 16 times higher than in natural sea-salt aerosols (SSA), indicating a strong Cl depletion phenomenon which was observed in the arctic atmosphere due to interaction of SSA with reactive gaseous species, mainly with NO*x* (or HNO3) (Gard et al., 1998; Geng et al., 2010). This is confirmed by the high concentration of nitrates NO_3^- ~ 80 ng/m^3, comparable with sulfates SO_4^{2-} while in the Arctic Ocean region the abundance of nitrates is usually lower than sulfates (Chang et al., 2011). Additionally, S, Fe, Na, Al, Si, Ca, Cl , K, Ti, Mn, Co, Cu, Zn, Ga, Sr, Ba, Hg, and Pb were detected above the LOD in background aerosols, sulfur concentration showed the largest mass concentration following by Fe, Na, and Al (Fig.S4).

When the wind was changed the pollution plume originating in the Tiksi urban area increased OC up to 2.1 $\mu g/m^3$ and added C=C-H (3041 cm^{-1}), -NO_2 (1507 cm^{-1}), and C-O (1052 cm^{-1}) groups to organic spectral features (Fig.8a), indicating polyaromatics, nitro- and oxygenated compounds (alcohols/esters) due to the episode of OC pollution. Since at that time EC concentrations were detected below LOD, therefore the pollution could be from the source with low BC production. Analyses of OC/EC ratio in urban environment (Samara et al., 2014) and from engine exhaust (Popovicheva et al., 2017b) shows that high-temperature traffic-related combustion associates to comparable EC and OC in ambient aerosols. Smoke of biomass burning (residential, agriculture and forest fires) in flaming phase is characterized by OC which concentration is less or comparable with EC, and only low-temperature pyrolysis (smoldering) produces a dominant amount of organic compounds (Popovicheva et al., 2015c; Reid et al., 2005).

Such finding for specific OC characteristics in the atmosphere near the CAF has initiated the focused search of the combustion sources for aerosol pollution in the Tiksi area. And, we found from the local media reports that waste burn events occurred at the landfill site which takes place to the west from the Tiksi settlement, see a map in Fig.1. Emphasizing that a landfill smoke plume could pass the CAF when the wind blew from the LPI sector, we propose that that local source which could generate aerosols with elevated OC and low EBC was the urban waste burning operating in slow smoldering phase.

OC pollution episode is associated with the sulfate mass increasing, up to 1.4 $\mu g/m^3$, which is composed of 90% non sea-salt sulfates (nss-SO_4^{2-}). It is related to a twofold increase of SO_4^{2-} absorption at 3232, 1144, 620 and 573 cm^{-1} (Fig.8a) in sulfuric acid and salts such as $(NH_4)_2SO_4$, $CaSO_4$, Na_2SO_4, and K_2SO_4, produced by heterogeneous reactions and secondary inorganic formation. Moreover, nss-SO_4^{2-} may

result from the reaction of SSA with sulfuric acid H_2SO_4 and methyl sulfonic acid CH_3SO_3H produced by oxidation of dimethyl sulfides CH_3SCH_3 of ocean biogenic emission. Vibrations at 1144 cm^{-1} observed in the FTIR spectrum of particles can be associated to organic sulfates such as RSO_2O^- in sulfonate salts, and R-$S(=O)_2$-R in sulfones (Fig.8a). It emphasizes the sulfur species production from marine source in the days when the wind blew from the Tiksi area taking place on the coast of Laptev sea. The wide nitrate band at 831 cm^{-1} indicates the Cl depletion in the polluted atmosphere where SSA acts as a sink for nitric acid and nitrogen oxides species (Graedel and Keene, 1995).

Nss-K^+ ions composed almost entire mass of K^+, near 200 ng/m^3, demonstrating the source of water-soluble potassium different from sea salt. It was shown that waste burning produce K^+ ions at concentration similar to biomass burning (Christian et al., 2010). Phosphate PO_4^{3-} ions were found at the high concentration of 160 ng/m^3 in comparison with negligible in background aerosols. They are detectable when plastics and garbage are burned in open fires, therefore phosphate were proposed as a specific tracer for plastics burning (Simoneit et al., 2005). Thus, we conclude that the waste burning was a possible source of K^+ and PO_4^{2-} ions in the aerosol composition during OC pollution episode.

Since 30 September EBC began to grow, its concentration was increased by 7 times during the BC pollution episode (Fig.4). At that time aerosols are characterized by elevated concentrations of aliphatic C-C-H, carboxylic acid C=O (1706 cm^{-1}), aldehydes C=O (1657 cm^{-1}), C-O (1074-1021 cm^{-1}), and NH_4^+, CO_3^{2-}, and SO_4^{2-} functional groups (Fig.8a). N-alkanes serve as a good indicator of BC urban and diesel emissions (Coury and Dillner, 2009; Popovicheva et al., 2015b). Anthropogenic and biomass burning organic material transported in the atmosphere tends to become more oxygenated due to secondary formation (Blando and Turpin, 2000; Popovicheva et al., 2016b). Ammonium nitrates and sulfates are known anthropogenic secondary species well correlating with oxygenated secondary species (Coury and Dillner, 2009). Thus, the change of aerosol composition observed is well identified by a pattern of functional markers which can be reasonably addressed to long - range transportation (LRT) from industrial and residential emission sources.

Significant increase of SO_4^{2-} mass concentrations, up to 1.6 $\mu g/m^3$, is correlated with the observation of sulfur 3 times higher during BC pollution episode (Fig.S4). Increase of the percent of SO_4^{2-} ions in total mass concentration from 50 to 70% indicates a strong influence of LRT from gas flaring, industrial and residential emission sources in Western Siberia, Krasnoyarsk Krai and Lena river delta (Fig.6a) which use sulfur-containing oil and diesel fuel therefore rich by sulfates (Klonecki et al., 2003). It worth to note that a layer of alkanes, organic-rich and scattering aerosols unambiguously attributed to anthropogenic emissions was observed at 4–6 km altitude (Warneke et al., 2010) where from air masses were descended to the HMO Tiksi at those days of BC pollution episodes. Additionally, we should note that volcano eruptions can impact the sulfate loading at the regional level. Intensive eruptions of the volcano in Kamchatka were observed at the beginning of September 2014 http://argumenti.ru/society/ 2014/09/363718. Forward trajectory at 30.09 to the Tiksi region clearly indicates the arrival from volcano Zhupanovskyi eruption at 4 km altitude.

Remarkably that the concentration of Cl^- ions was also found unusually high during this pollution episode, up to 200 ng/m^3. Thus, Na^+/Cl^- ratio approached 1, in opposite to the phenomenon of the Cl depletion. Probably, residential and waste burning in regions of Krasnoyarsk Krai generated HCl emissions which is known as globally making a major source of soluble Cl^- (Christian et al., 2010). And ammonium NH_4^+ approached 195 ng/m^3, according to increased SO_4^{2-} , as secondary inorganic aerosol species.

Observations in **September 2015** showed the similar high concentration of OC, above 2 μg/m^3, (Fig.7a) with aliphatic, oxygenated compounds and ammonium dominated the aerosol composition (Fig.8b). Since at that time the wind from the LPI sector was frequent we can assume that high OC was carried by a smoke plume from the landfill continuously burning in the Tiksi area, well in correlation with K^+, Cl^-, and PO_4^{3-} ions distinguishable as markers of waste burning. It increased Cl^- concentration, thus the ratio Na^+/Cl^- on average was 1.6, still indicating a Cl depletion phenomenon but not such prominent in comparison with background period.

During the BC pollution episode (Fig.4), related to the largest impact from local urban emissions, the absorption features showed the significant increase of carbonyl groups relating to esters/lactones in the aerosol composition (Fig.8a). However, concentrations of SO_4^{2-} and NH_4^+**, ~** 500 and 40 ng/m^3, respectively, were observed significantly lower than in 2014. More frequent west wind occurred at that time which decreased the impact of regional sources of secondary sulfate and ammonium formation from the continent while increased the genuine sea-salts production from the ocean, indicated by hydroxyls at 3560 cm^{-1} (Fig.8b).

Aerosol composition data collected **in September 2016** are the most difficult for interpretation because of the frequently repeated episodes of increased EBC (Fig.4). OC mass concentrations, near 3.5 μg/m^3, occurred, even higher than in previous sampling periods, indicating a strong impact of continuously running source of prominent organic emission. Since such pollution is appeared to be reproducible in September we repeated the visual inspection of the area around the HMO and found the smoke plume from the landfill site spreading from the Tiksi settlement, a photo taken on 15.09 is shown in Fig.1. At that time the smoldering combustion phase made the significant contribution: white smoke was dominant on the landfill site.

OC pollution brought aliphatic, ester/lactones (1740 cm^{-1}), and acids/ketones (1710 cm^{-1}) to aerosol composition as well as aromatic compounds observed during the whole sampling period of September 2016 as the specific spectral absorption C=C-H and C=C bands at 3064 and 1617 cm^{-1}, respectively (Fig.8b). Since BC pollution episode was happened at that time related to the wind from the marine habour, the influence of ship traffic on aerosol chemistry in the surrounding ocean should be emphasized, as observed in (Xie et al., 2007). Alkanes, esters, and polyaromatic compounds were found in ship exhaust residuals (Popovicheva et al., 2009) which are well recognized as functional markers of on-road and off-road diesel emission (Popovicheva et al., 2015b). Organic matter concentration and functional group composition measured at the

Barrow station in autumn months had 4-day averaged OM concentrations below 500 ng/m^3 and consisted of about half alkane and half hydroxyl group fractions (Shaw et al., 2010).

Moreover, the total concentration of water-soluble ions approached 3.5 μg/m^3 in that period, a maximum value between other September periods. It was dominated by sulfate secondary formation due to LRT from central Yakutia as well as from Tiksi urban area where the local power plant, heating stations, and diesel and marine transport use rare oil and sulfur-containing fuel. Because one episode of increased EBC was impacted by local urban sources while the LRT of polluted air masses from central Yakutia related to two other episodes we conclude that both OC and BC pollution episodes demonstrate the features of waste burning and fossil fuel combustion from both local and regional sources. At that time the ratio Na^+/Cl^- was 3.08±0.8 on average, indicating the consistent Cl depletion phenomenon in the BC polluted atmosphere.

3.2.2. Winter – spring.

Anthropogenic emissions from northern Eurasia are identified by surface, airborne, and remote sensing measurements as the principal source for seasonal atmospheric background of the Arctic Haze (Law and Stohl, 2007). It is also expected for East Siberian Arctic aerosols on the coast of Laptev sea.

Polar night in the Tiksi region lasts from 19 November to 24 January therefore winter sampling **in November 2014** took place during sunlight absence time, when temperature dropped down to minimum -31^0 C (Table 1). On average, OC was on average 0.97 ± 0.33 μg/m^3, less than in autumn aerosols. For comparison, the OC burden at the Barrow station was 0.33 ± 0.07 ng/m^3 in winter (Barrett et al., 2015). Organic functional groups during the sampling period show a big similarity of aerosol composition. They are distinguished by the strong carbonyl (1702 cm^{-1}) but low aliphatic (2856 cm^{-1}) and aromatic (3063 cm^{-1}) bands for all sampling days, including of highest EBC (Fig.8c). November aerosols are found different from September ones by much higher abundance of oxygenated compounds with respect to alkanes, by 68 times, as determined by the ratio C=O/C-C-H of peak area bands. All sampling days were under strongest influence of consistent LRT from central Yakutia therefore a substantial portion of dicarboxylic acids/ketones was likely derived from atmospheric oxidation of transported particulate matter. Such phenomenon of substantial increase in water-soluble organics, including dicarboxylic acids, ketoacids, α-dicarbonyls, and sugars was observed for particles arrived from Siberia to Pacific Ocean (Agarwal et al., 2010) and can exhibit the processes of chemical transformation during the aging of aerosol emission in the atmosphere. Prominent absorption of ammonium (3247 cm^{-1}) and sulfates (704 cm^{-1}) demonstrates the high impact of secondary inorganic aerosol formation and transportation to Laptev sea region, mixed with silicate ions SiO_4^{4-} (978 cm^{-1}) in various aluminosilicates and carbonates (874, 1428 cm^{-1}) in dust (Fig.8c).

November aerosols are characterized by increased total ion and sulfate mass concentrations in comparison with September ones, well with a general trend of the aerosol mass increase in the Arctic in winter. On average, SO_4^{2-} was 1.79 ± 0.43 μg/m^3, higher than OC following a tendency which is typically observed for sulfates during the Arctic Haze. It indicates that the particles emitted from primary sources

aged in the atmosphere and have gained secondary sulfates either through coagulation with atmospheric sulfates, cloud processing, and heterogeneous oxidation of SO_2 (Yun et al., 2013). High NH_4^+, on average 0.22±0.16 μg/m^3 was related to a winter tendency of sulfates. The averaged ratio Na^+/Cl^- ~ 0.74 indicated either natural SSA or a Cl depletion phenomenon compensated in chlorine highly - polluted atmosphere, the last is more probable because NO_3^- concentration approached high value of 410 ng/m^3 at that time.

The most severe air pollution was happened during **March 2015** sampling period when the concentrations of sulfates and total ions exceeded the previously recorded maxima, up to 3.7 and 6 μg/m^3, respectively. OC also showed higher values then in November, on average 2.1±0.3 μg/m^3. Air mass transport from lower latitudes of central Yakutia was consistent at that time, remaining organic composition to be similar to November one, also distinguished by the strong carbonyl and low aliphatic functional groups (Fig.8c). Nss-K^+ ions approached the highest value of 580 ng/m^3. Being ionic marker of biomass burning (Popovicheva et al., 2016a) they demonstrate the impact of residential biomass burning.

During the BC pollution episode ammonium and sulfates become less prominent (Fig.8c) coming from the LPI sector at that time. For comparison, at the Barrow station aerosols during spring months had daily-averaged organic matter concentrations higher than 1 μg/m^3 and consisted of approximately half alkane groups with the other half split between carboxylic acid and hydroxyl groups (Shaw et al., 2010). Abundance of carbohydrate-like hydroxyls were associated to organic-salt coatings raised during sea ice formation. However, hydroxyls were not observed in aerosol composition of spring sampling at HMO Tiksi probably because low impact of ocean-derived sources as the dominant wind at that time was happen from west and north while air mass transportation was from the continent.

As sunlight returns in spring, the solar radiation provides favorable conditions for the enhancement of the reaction of NO*x* (or HNO_3) and SSA. (Gard et al., 1998) observed that such active heterogeneous chemical reactions primarily occurred during the daytime, they were completely converted SSA mostly into $NaNO_3$ particles. At Ny-Ålesund, the all-day-long daytime during the spring period enhanced photochemical activities, consequently resulting in the production of nitric acid that readily reacts with sea-salt particles (Geng et al., 2010). However, during the sampling days in March 2015 the averaged ratio Na^+/Cl^- was just 0.7, near SSA composition as in November. Furthermore, it is suggested by Fenger et al. (2012) that Cl^- containing particles at Station Nord could be originated from frost flowers torn at high wind speeds. Thus, both frost flowers and the marine snow pack near HMO Tiksi can be sources of sea salt.

In contrast to the Arctic Haze period, summer months are much cleaner due to stronger blocking of the pollutant transport into the Arctic (Quinn et al., 2008). In **May-June 2015** when the tundra became snow-free, the background and BC pollution episode qualitatively repeated the ones in September 2014 (Fig.4). In the background period OC originated from biogenic and marine activity was low, around ~ 800 ng/m^3, and characterized by the similar pattern of functionalities as was observed in September: by hydroxyl C-OH (3470 cm^{-1}), amino N-H/ammonium NH_4^+ (3218 cm^{-1}), carbonyl C=O (1710 cm^{-1}), -NO_2 (1539 cm^{-1}), NO_3^- (815 cm^{-1}), and SO_4^{2-} (681, 588 cm^{-1}) groups with negligible aliphatic compounds (Fig.8d). Strong increase

of aliphatic C-C-H (2908-2841 cm^{-1}) with additional SO_4^{2-} (704 cm^{-1}) was relevant to the BC pollution episode associated with the emission impact from the LPI sector of adjusted Tiksi urban area because alkanes are associated to dominated functionalities of diesel emissions (Popovicheva et al., 2015a).

Sampling period of **June 2016** was different from 2015 by a rapid change of aerosol chemistry related to strong EBC variations almost each day. OC was found as high as 2.83 and 2.44 $\mu g/m^3$ on 04-05.06 and 07-8.06, respectively, at those days when air mass trajectories passed through large areas of intensive agricultural burning and wildfires observed in central and western Siberia and on Yamal peninsula. The reason for such high OC observed could be photochemical and physical aging processes during long-range transport of fire plumes when condensation and cloud processing of semi-volatile organic compounds tend to increase OC in particulate matter (Konovalov et al., 2015). Much higher abundance of acid and non-acid (1719 cm^{-1}) functional groups in carboxylic acids and ketones, respectively, is distinguished by 4 times with respect to alkanes in OC polluted aerosols (Fig.8e). Non-acidic carbonyls in addition to carboxylic acid groups were found as the functional marker of forest fire emissions and were assigned to aldehyde/ketone, ester/lactone, and acid anhydride groups (Hawkins and Russell, 2010). Specific spectral absorption observed during those days when OC pollution correlates with highly increased EBC is prominent aromatic C=C bands at 1594 cm^{-1}, respectively, which is related to diesel transport emission as well as shipping in local sources.

At Ny-Alesund station the presence of spring-to-summer switch was confirmed by the reduction of the seasonal average of the nss-SO_2^{4-} daily concentrations by 91% (Bazzano et al., 2015). The similar trend is observed during our yearly summer sampling periods. In May-June 2015 and June 2016 mass concentrations of sulfates averaged over the sampling period was decreased by 82 and 87% in comparison with maximum observed in March 2015. SO_4^{2-} ions no more dominate the ion composition, sea salts, potassium, nitrates, ammonium, and calcium make up the aerosol inorganic mass in early summer. In days of high OC K^+ ions approached 302 ng/m^3, confirming the strong influence of wildfires on the local aerosol burden.

4. Conclusions.

The long - time gap in aerosol observations in the Siberian Arctic strongly limited the estimations of rapid climate forcing. This work provides the opportunity in quantification of East Siberian Arctic background and black carbon polluted aerosols, the source and season impacts on their concentrations and composition done by comprehensive characterization of aerosol optical and physico-chemical properties. It is shown that the Hydrometeorological Observatory (HMO) Tiksi surrounded by the Arctic Ocean from one side and by the continent from other side, is affected by both marine, biogenic and anthropogenic sources from lower latitudes as well as influenced by local emissions. EBC time series analysis during two years of observations indicates that EBC concentrations undergo the frequent variations imposed upon the seasonal trends. Aerosol sampling of one-three days better resolves the irregular episodes of increased EBC which bring the extensive amount of pollutants to arctic aerosols. Chemical characterization of aerosols performed

at HMO Tiksi is highly valuable for evaluation of episodes of increased EBC as the events of anthropogeneous pollution due to long-range air mass transport from lower latitudes in Siberia and emissions from adjacent urban area. Focus on source-dependent aerosol characteristics during EBC pollution episodes combined with the analyses of wind direction and air mass transportation allows the quantification of the pollution with respect to background. Since the times for sampling campaigns were arbitrary we can put the observations of the background and BC pollution episodes in the context of the long - term BC variability and conclude that two year EBC monitoring at the HMO Tiksi in September shows quite well repeatability with respect to relatively frequent pollution events, thus giving us the opportunity to analyze both the background arctic aerosols and polluted ones from the point of view of the increased BC concentration.

In September, the major components of background aerosols are characterized by low EBC, alkanes, carboxylic acids/ketones, aminocompounds, and saccharides, as well as organic and inorganic sulfates, sea salts, and windblown dust. The reason for a lack of Cl^- is the chemical transformation of sea-salt in the atmosphere polluted by nitrogen oxides. High sulfate concentrations in September originate from biological activity near the coast of Laptev sea and secondary sulfate formation. Increased mass concentrations of EBC and SO_4^{2-} indicate the combustion emission, in accordance with the abundance of aliphatic and carbonyls as functional markers of urban and industrial sources identified by the long-range air masses transport from gas flaring, industrial, and residential regions in Western Siberia, Krasnoyarsk Krai, and Central Yakutia. Ionic markers for waste burning PO_4^{3-}, K^+, and Cl^- supports the identification of the Tiksi city landfill plumes carrying the hazardous compounds. Reproduction of high OC concentrations in September of both 2014, 2015, and 2016 years demonstrates that municipal waste burning could be an intensive local source of atmospheric pollution at the HMO Tiksi.

Elevated EBC, sulfates, and OC during the winter and spring are a result of the intensification of meridional transport from the midlatitudes to the Arctic as well as of high stability of the atmospheric surface layer leading to the increase of both the background and pollution level. Organic aerosols of the Arctic Haze are composed almost from carboxylic acid and alkanes indicating that not only mass concentrations are enhanced within the Arctic troposphere but also aerosol chemistry is changing under long-range air mass transportation from low latitudes. In early summer, less pollutant transport into the Arctic decrease the mass concentrations of EBC and sulfates almost to the level of early autumn. However, wildfire events in Siberia impact to increased OC dominated by highly - oxidized acid compounds. BC pollution episodes are connected with local emissions originating in industrial, traffic, and harbor activities indicated by markers of diesel transport and shipping emissions.

This study firstly quantifies the BC-polluted aerosols during sampling periods at the HMO Tiksi by comprehensive analyses of atmospheric particle chemistry combined with meteorological parameter, stratification of the boundary layer and air mass transportation. It is supported by the identification of source-specific chemical, functional and ionic markers and increases the state of scientific understanding for aerosol/climate interactions and dangerous impacts on climate. Therefore, further strategy for understanding,

documenting, and identifying the local and regional origin of Arctic air pollution episodes in the vastly understudied Siberian Arctic should be developed. Although at present there are few high Arctic sources of BC, emissions are expected to grow due to increased human activity in the Arctic, therefore demanding special attention to the local sources of pollution.

Acknowledgement. Financial support from RFBR– project , Roshydromet CNTP project 1.5.3.2 and EnTeC FP7 Capacities Programme (REGPOT-2012-2013-1, FP7, ID: 316173) is acknowledged. Authors thank to Dr. P. Bogorodski (AARI) for performance of sampling at HMO Tiksi.

References.

Agarwal, S., Aggarwal, S.G., Okuzawa, K., Kawamura, K., 2010. Size distributions of dicarboxylic acids, ketoacids, α-dicarbonyls, sugars, WSOC, OC, EC and inorganic ions in atmospheric particles over Northern Japan: implication for long-range transport of Siberian biomass burning and East Asian polluted aerosols. Atmospheric Chemistry and Physics 10, 5839-5858.

Asmi, E., Kondratyev, V., Brus, D., Laurila, T., Lihavainen, H., Backman, J., Vakkari, V., Aurela, M., Hatakka, J., Viisanen, Y., Uttal, T., Ivakhov, V., Makshtas, A., 2016. Aerosol size distribution seasonal characteristics measured in Tiksi, Russian Arctic. Atmos. Chem. Phys. 16, 1271-1287.

Barrett, T.E., Robinson, E.M., Usenko, S., Sheesley, R.J., 2015. Source Contributions to Wintertime Elemental and Organic Carbon in the Western Arctic Based on Radiocarbon and Tracer Apportionment. Environmental Science & Technology 49, 11631-11639.

Baumgardner, D., Popovicheva, O., Allan, J., Bernardoni, V., Cao, J., Cavalli, F., Cozic, J., Diapouli, E., Eleftheriadis, K., Genberg, P., 2012. Soot reference materials for instrument calibration and intercomparisons: a workshop summary with recommendations. Atmospheric Measurement Techniques 5, 1869-1887.

Bazzano, A., Ardini, F., Becagli, S., Traversi, R., Udisti, R., Cappelletti, D., Grotti, M., 2015. Source assessment of atmospheric lead measured at Ny-Ålesund, Svalbard. Atmospheric Environment 113, 20-26.

Blando, J.D., Turpin, B.J., 2000. Secondary organic aerosol formation in cloud and fog droplets: a literature evaluation of plausibility. Atmospheric Environment 34, 1623-1632.

Brock, C.A., Cozic, J., Bahreini, R., Froyd, K.D., Middlebrook, A.M., McComiskey, A., Brioude, J., Cooper, O., Stohl, A., Aikin, K., 2011. Characteristics, sources, and transport of aerosols measured in spring 2008 during the aerosol, radiation, and cloud processes affecting Arctic Climate (ARCPAC) Project. Atmospheric Chemistry and Physics 11, 2423-2453.

Cavalli, F., Viana, M., Yttri, K.E., Genberg, J., Putaud, J.P., 2010. Toward a standardised thermal-optical protocol for measuring atmospheric organic and elemental carbon: the EUSAAR protocol. Atmos. Meas. Tech. 3, 79-89.

Chang, R.-W., Leck, C., Graus, M., Müller, M., Paatero, J., Burkhart, J.F., Stohl, A., Orr, L., Hayden, K., Li, S.-M., 2011. Aerosol composition and sources in the central Arctic Ocean during ASCOS.

Christian, T.J., Yokelson, R., Cárdenas, B., Molina, L., Engling, G., Hsu, S.-C., 2010. Trace gas and particle emissions from domestic and industrial biofuel use and garbage burning in central Mexico. Atmospheric Chemistry and Physics 10, 565-584.

Coury, C., Dillner, A.M., 2009. ATR-FTIR characterization of organic functional groups and inorganic ions in ambient aerosols at a rural site. Atmospheric Environment 43, 940-948.

Eckhardt, S., Quennehen, B., Olivié, D.J.L., Berntsen, T.K., Cherian, R., Christensen, J.H., Collins, W., Crepinsek, S., Daskalakis, N., Flanner, M., Herber, A., Heyes, C., Hodnebrog, Ø., Huang, L., Kanakidou, M., Klimont, Z., Langner, J., Law, K.S., Lund, M.T., Mahmood, R., Massling, A., Myriokefalitakis, S., Nielsen, I.E., Nøjgaard, J.K., Quaas, J., Quinn, P.K., Raut, J.C., Rumbold, S.T., Schulz, M., Sharma, S., Skeie, R.B., Skov, H., Uttal, T., von Salzen, K., Stohl, A., 2015. Current model capabilities for simulating black carbon

and sulfate concentrations in the Arctic atmosphere: a multi-model evaluation using a comprehensive measurement data set. Atmos. Chem. Phys. 15, 9413-9433.
Eleftheriadis, K., Nyeki, S., Psomiadou, C., Colbeck, I., 2004. Background aerosol properties in the European arctic. Water, Air and Soil Pollution: Focus 4, 23-30.
Eleftheriadis, K., Vratolis, S., Nyeki, S., 2009. Aerosol black carbon in the European Arctic: Measurements at Zeppelin station, Ny-Ålesund, Svalbard from 1998–2007. Geophysical Research Letters 36, n/a-n/a.
Flanner, M.G., 2013. Arctic climate sensitivity to local black carbon. Journal of Geophysical Research: Atmospheres 118, 1840-1851.
Frossard, A.A., Russell, L.M., Burrows, S.M., Elliott, S.M., Bates, T.S., Quinn, P.K., 2014. Sources and composition of submicron organic mass in marine aerosol particles. Journal of Geophysical Research: Atmospheres 119.
Fu, P., Kawamura, K., Barrie, L.A., 2009. Photochemical and Other Sources of Organic Compounds in the Canadian High Arctic Aerosol Pollution during Winter−Spring. Environmental Science & Technology 43, 286-292.
Gard, E.E., Kleeman, M.J., Gross, D.S., Hughes, L.S., Allen, J.O., Morrical, B.D., Fergenson, D.P., Dienes, T., Gälli, M.E., Johnson, R.J., 1998. Direct observation of heterogeneous chemistry in the atmosphere. Science 279, 1184-1187.
Geng, H., Ryu, J., Jung, H.-J., Chung, H., Ahn, K.-H., Ro, C.-U., 2010. Single-particle characterization of summertime Arctic aerosols collected at Ny-Ålesund, Svalbard. Environmental science & technology 44, 2348-2353.
Graedel, T., Keene, W., 1995. Tropospheric budget of reactive chlorine. Global Biogeochemical Cycles 9, 47-77.
Hawkins, L.N., Russell, L.M., 2010. Oxidation of ketone groups in transported biomass burning aerosol from the 2008 Northern California Lightning Series fires. Atmospheric Environment 44, 4142-4154.
Hirdman, D., Sodemann, H., Eckhardt, S., Burkhart, J.F., Jefferson, A., Mefford, T., Quinn, P.K., Sharma, S., Ström, J., Stohl, A., 2010. Source identification of short-lived air pollutants in the Arctic using statistical analysis of measurement data and particle dispersion model output. Atmos. Chem. Phys. 10, 669-693.
Huang, K., Fu, J.S., Prikhodko, V.Y., Storey, J.M., Romanov, A., Hodson, E.L., Cresko, J., Morozova, I., Ignatieva, Y., Cabaniss, J., 2015. Russian anthropogenic black carbon: Emission reconstruction and Arctic black carbon simulation. Journal of Geophysical Research: Atmospheres 120.
Klonecki, A., Hess, P., Emmons, L., Smith, L., Orlando, J., Blake, D., 2003. Seasonal changes in the transport of pollutants into the Arctic troposphere-model study. Journal of Geophysical Research: Atmospheres 108.
Konovalov, I., Beekmann, M., Berezin, E., Petetin, H., Mielonen, T., Kuznetsova, I., Andreae, M., 2015. The role of semi-volatile organic compounds in the mesoscale evolution of biomass burning aerosol: a modeling case study of the 2010 mega-fire event in Russia. Atmospheric Chemistry and Physics 15, 13269-13297.
Law, K.S., Stohl, A., 2007. Arctic air pollution: Origins and impacts. science 315, 1537-1540.
Li, S.-M., Winchester, J.W., 1989. Resolution of ionic components of late winter arctic aerosols. Atmospheric Environment (1967) 23, 2387-2399.
Makarov, V., Fukasawa, T., Ohta, S., 2007. Variation of atmospheric aerosol carbon concentration in Yakutia Journal of global environment engineering 12, 87-96.
Makshtas, A.P., B.V. Ivanov, V.F. Timachev 2012. Comparison of universal functions of stability in conditions of strong stable-stratified atmosphere. Problemy Arktiki i Antarktiki 3, 5-16.
Maria, S.F., Russell, L.M., Turpin, B.J., Porcja, R.J., 2002. FTIR measurements of functional groups and organic mass in aerosol samples over the Caribbean. Atmospheric Environment 36, 5185-5196.
Mikhailov, E.F., Mironova, S., Mironov, G., Vlasenko, S., Panov, A., Chi, X., Walter, D., Carbone, S., Artaxo, P., Heimann, M., 2017. Long-term measurements (2010–2014) of carbonaceous aerosol and carbon monoxide at the Zotino Tall Tower Observatory (ZOTTO) in central Siberia. Atmospheric Chemistry and Physics 17, 14365-14392.
Nguyen, Q.T., Skov, H., Sørensen, L.L., Jensen, B.J., Grube, A.G., Massling, A., Glasius, M., Nøjgaard, J.K., 2013. Source apportionment of particles at Station Nord, North East Greenland during 2008–2010 using COPREM and PMF analysis. Atmos. Chem. Phys. 13, 35-49.
Popovicheva, O., Engling, G., Lin, K.-T., Persiantseva, N., Timofeev, M., Kireeva, E., Völk, P., Hubert, A., Wachtmeister, G., 2015a. Diesel/biofuel exhaust particles from modern internal combustion engines: microstructure, composition, and hygroscopicity. Fuel 157, 232-239.

Popovicheva, O., Kireeva, E., Shonija, N., Zubareva, N., Persiantseva, N., Tishkova, V., Demirdjian, B., Moldanová, J., Mogilnikov, V., 2009. Ship particulate pollutants: Characterization in terms of environmental implication. Journal of Environmental Monitoring 11, 2077-2086.

Popovicheva, O.B., Engling, G., Diapouli, E., Saraga, D., Persiantseva, N.M., Timofeev, M., Kireeva, E.D., Shonija, N.K., Chen, S.-H., Nguyen, D.L., 2016a. Impact of smoke intensity on size-resolved aerosol composition and microstructure during the biomass burning season in Northwest Vietnam. Aerosol and Air Quality Research 16, 2635-2654.

Popovicheva, O.B., Engling, G., Diapouli, E., Saraga, D., Persiantseva, N.M., Timofeev, M.A., Kireeva, E.D., Shonija, N.K., Chen, S.-H., Nguyen, D.-L., Eleftheriadis, K., Lee, C.-T., 2016b. Impact of Smoke Intensity on Size-Resolved Aerosol Composition and Microstructure during the Biomass Burning Season in Northwest Vietnam. Aerosol Air Quality Research 16, 2635-3654.

Popovicheva, O.B., Evangeliou, N., Eleftheriadis, K., Kalogridis, A.C., Sitnikov, N., Eckhardt, S., Stohl, A., 2017a. Black Carbon Sources Constrained by Observations in the Russian High Arctic. Environmental Science & Technology 51, 3871-3879.

Popovicheva, O.B., Irimiea, C., Carpentier, Y., Ortega, I.K., Kireeva, E.D., Shonija, N.K., Schwarz, J., Vojtíšek-Lom, M., Focsa, C., 2017b. Chemical Composition of Diesel/Biodiesel Particulate Exhaust by FTIR Spectroscopy and Mass Spectrometry: Impact of Fuel and Driving Cycle. Aerosol and Air Quality Research 17, 1717-1734+ ap1711.

Popovicheva, O.B., Kireeva, E.D., Shonija, N.K., Vojtisek-Lom, M., Schwarz, J., 2015b. FTIR analysis of surface functionalities on particulate matter produced by off-road diesel engines operating on diesel and biofuel. Environmental Science and Pollution Research 22, 4534-4544.

Popovicheva, O.B., Kozlov, V.S., Engling, G., Diapouli, E., Persiantseva, N.M., Timofeev, M., Fan, T.-S., Saraga, D., Eleftheriadis, K., 2015c. Small-scale study of Siberian biomass burning: I. Smoke microstructure. Aerosol Air Qual. Res 15, 117-128.

Quinn, P., Shaw, G., Andrews, E., Dutton, E., Ruoho-Airola, T., Gong, S., 2007. Arctic haze: current trends and knowledge gaps. Tellus B 59, 99-114.

Quinn, P.K., Bates, T.S., Baum, E., Doubleday, N., Fiore, A.M., Flanner, M., Fridlind, A., Garrett, T.J., Koch, D., Menon, S., Shindell, D., Stohl, A., Warren, S.G., 2008. Short-lived pollutants in the Arctic: their climate impact and possible mitigation strategies. Atmos. Chem. Phys. 8, 1723-1735.

Rahn, K.A., Tomza, U., Khodzher, T., 1997. An event of long-range transport of Siberian aerosol to Tiksi, Russia. Journal of Aerosol Science 28, S465-S466.

Reid, J.S., Koppmann, R., Eck, T.F., Eleuterio, D.P., 2005. A review of biomass burning emissions part II: intensive physical properties of biomass burning particles. Atmospheric Chemistry and Physics 5, 799-825.

Russell, L.M., Hawkins, L.N., Frossard, A.A., Quinn, P.K., Bates, T.S., 2010. Carbohydrate-like composition of submicron atmospheric particles and their production from ocean bubble bursting. Proceedings of the National Academy of Sciences 107, 6652-6657.

Sakerin, S., Chernov, D., Kabanov, D., Kozlov, V., Panchenko, M., Polkin, V., Radionov, V., 2012. Preliminary results of studying the aerosol characteristics of the atmosphere in the region of Barentsburg, Spitsbergen. Problemi Arktiki i Antarktiki 1, 20-31.

Sakerin, S.M., Bobrikov, A.A., Bukin, O.A., Golobokova, L.P., Pol'kin, V.V., Pol'kin, V.V., Shmirko, K.A., Kabanov, D.M., Khodzher, T.V., Onischuk, N.A., Pavlov, A.N., Potemkin, V.L., Radionov, V.F., 2015. On measurements of aerosol-gas composition of the atmosphere during two expeditions in 2013 along the Northern Sea Route. Atmos. Chem. Phys. 15, 12413-12443.

Samara, C., Voutsa, D., Kouras, A., Eleftheriadis, K., Maggos, T., Saraga, D., Petrakakis, M., 2014. Organic and elemental carbon associated to PM 10 and PM 2.5 at urban sites of northern Greece. Environmental Science and Pollution Research 21, 1769-1785.

Sharma, S., Ishizawa, M., Chan, D., Lavoué, D., Andrews, E., Eleftheriadis, K., Maksyutov, S., 2013. 16-year simulation of Arctic black carbon: Transport, source contribution, and sensitivity analysis on deposition. Journal of Geophysical Research: Atmospheres 118, 943-964.

Sharma, S., Lavoué, D., Cachier, H., Barrie, L., Gong, S., 2004. Long-term trends of the black carbon concentrations in the Canadian Arctic. Journal of Geophysical Research: Atmospheres 109.

Shaw, P., Russell, L., Jefferson, A., Quinn, P., 2010. Arctic organic aerosol measurements show particles from mixed combustion in spring haze and from frost flowers in winter. Geophysical Research Letters 37.

Shindell, D., Faluvegi, G., 2009. Climate response to regional radiative forcing during the twentieth century. Nature Geoscience 2, 294.
Simoneit, B.R., Medeiros, P.M., Didyk, B.M., 2005. Combustion products of plastics as indicators for refuse burning in the atmosphere. Environmental science & technology 39, 6961-6970.
Stein, A., Draxler, R., Rolph, G., Stunder, B., Cohen, M., Ngan, F., 2015. NOAA's HYSPLIT atmospheric transport and dispersion modeling system, B. Am. Meteorol. Soc., 96, 2059–2077.
Stock, M., Ritter, C., Herber, A., von Hoyningen-Huene, W., Baibakov, K., Gräser, J., Orgis, T., Treffeisen, R., Zinoviev, N., Makshtas, A., Dethloff, K., 2012. Springtime Arctic aerosol: Smoke versus haze, a case study for March 2008. Atmospheric Environment 52, 48-55.
Stohl, A., 2006. Characteristics of atmospheric transport into the Arctic troposphere. Journal of Geophysical Research: Atmospheres 111, n/a-n/a.
Stohl, A., Berg, T., Burkhart, J., Fjæraa, A., Forster, C., Herber, A., Hov, Ø., Lunder, C., McMillan, W., Oltmans, S., 2007. Arctic smoke–record high air pollution levels in the European Arctic due to agricultural fires in Eastern Europe in spring 2006. Atmospheric Chemistry and Physics 7, 511-534.
Stohl, A., Klimont, Z., Eckhardt, S., Kupiainen, K., Shevchenko, V.P., Kopeikin, V.M., Novigatsky, A.N., 2013. Black carbon in the Arctic: the underestimated role of gas flaring and residential combustion emissions. Atmos. Chem. Phys. 13, 8833-8855.
Stone, R.S., Sharma, S., Herber, A., Eleftheriadis, K., Nelson, D.W., 2014. A characterization of Arctic aerosols on the basis of aerosol optical depth and black carbon measurements. Elem Sci Anth 2.
Tomasi, C., Vitale, V., Lupi, A., Di Carmine, C., Campanelli, M., Herber, A., Treffeisen, R., Stone, R.S., Andrews, E., Sharma, S., Radionov, V., von Hoyningen-Huene, W., Stebel, K., Hansen, G.H., Myhre, C.L., Wehrli, C., Aaltonen, V., Lihavainen, H., Virkkula, A., Hillamo, R., Ström, J., Toledano, C., Cachorro, V.E., Ortiz, P., de Frutos, A.M., Blindheim, S., Frioud, M., Gausa, M., Zielinski, T., Petelski, T., Yamanouchi, T., 2007. Aerosols in polar regions: A historical overview based on optical depth and in situ observations. Journal of Geophysical Research: Atmospheres 112, n/a-n/a.
Treffeisen, R., Turnved, P., StrÖm, J., Herber, A., Bareiss, J., Helbig, A., Stone, R.S., Hoyningen-Huene, W., Krejci, R., Stohl, A., Neuber, R., 2007. Arctic smoke ? aerosol characteristics during a record air pollution event in the European Arctic and its radiative impact. Atmospheric Chemistry and Physics Discussions 7, 2275-2324.
Trentmann, J., Luderer, G., Winterrath, T., Fromm, M., Servranckx, R., Textor, C., Herzog, M., Graf, H.-F., Andreae, M., 2006. Modeling of biomass smoke injection into the lower stratosphere by a large forest fire (Part I): reference simulation. Atmospheric Chemistry and Physics 6, 5247-5260.
Uttal, T., Makshtas, A., Laurila, T., 2013. The Tiksi International Hydrometeorological Observatory-An Arctic Members Partnership. WMO Bull. 62, 22-26.
von Schneidemesser, E., Schauer, J.J., Hagler, G.S.W., Bergin, M.H., 2009. Concentrations and sources of carbonaceous aerosol in the atmosphere of Summit, Greenland. Atmospheric Environment 43, 4155-4162.
Wang, Q., Jacob, D.J., Fisher, J.A., Mao, J., Leibensperger, E.M., Carouge, C.C., Le Sager, P., Kondo, Y., Jimenez, J.L., Cubison, M.J., Doherty, S.J., 2011. Sources of carbonaceous aerosols and deposited black carbon in the Arctic in winter-spring: implications for radiative forcing. Atmos. Chem. Phys. 11, 12453-12473.
Warneke, C., Froyd, K., Brioude, J., Bahreini, R., Brock, C., Cozic, J., De Gouw, J., Fahey, D., Ferrare, R., Holloway, J., 2010. An important contribution to springtime Arctic aerosol from biomass burning in Russia. Geophysical Research Letters 37.
Winiger, P., Andersson, A., Eckhardt, S., Stohl, A., Semiletov, I.P., Dudarev, O.V., Charkin, A., Shakhova, N., Klimont, Z., Heyes, C., Gustafsson, Ö., 2017. Siberian Arctic black carbon sources constrained by model and observation. Proceedings of the National Academy of Sciences 114, E1054-E1061.
Xie, Z., Blum, J.D., Utsunomiya, S., Ewing, R., Wang, X., Sun, L., 2007. Summertime carbonaceous aerosols collected in the marine boundary layer of the Arctic Ocean. Journal of Geophysical Research: Atmospheres 112.
Yin, F., Grosjean, D., Flagan, R.C., Seinfeld, J.H., 1990. Photooxidation of dimethyl sulfide and dimethyl disulfide. II: Mechanism evaluation. Journal of Atmospheric Chemistry 11, 365-399.
Yun, Y., Penner, J.E., Popovicheva, O., 2013. The effects of hygroscopicity on ice nucleation of fossil fuel combustion aerosols in mixed-phase clouds. Atmos. Chem. Phys. 13, 4339-4348.

Zhang, Z.S., Engling, G., Chan, C.Y., Yang, Y.H., Lin, M., Shi, S., He, J., Li, Y.D., Wang, X.M., 2013. Determination of isoprene-derived secondary organic aerosol tracers (2-methyltetrols) by HPAEC-PAD: Results from size-resolved aerosols in a tropical rainforest. Atmospheric Environment 70, 468-476.

Highlights.

Observations of black carbon, organics, and sulfates in East Siberian Arctic aerosols

Highly-oxygenated organic compounds and ionic markers are the specific feature of aerosol chemistry relating to urban pollution.

Chemical speciation of arctic BC-polluted aerosol with respect to chemical markers and assessment of source contribution.

Carbon fractions (OC, EC), organic and inorganic functional groups, and ions characterize the arctic background and pollution episodes.

Identification of increasing the aerosol pollutant components establishes the relation between the aerosol composition and BC-polluted environment supported by low wind speed, stable stratification of the boundary layer, and long transportation.

Complementary insight on source-influenced and season-dependent composition of East Siberian Arctic aerosols.

a)

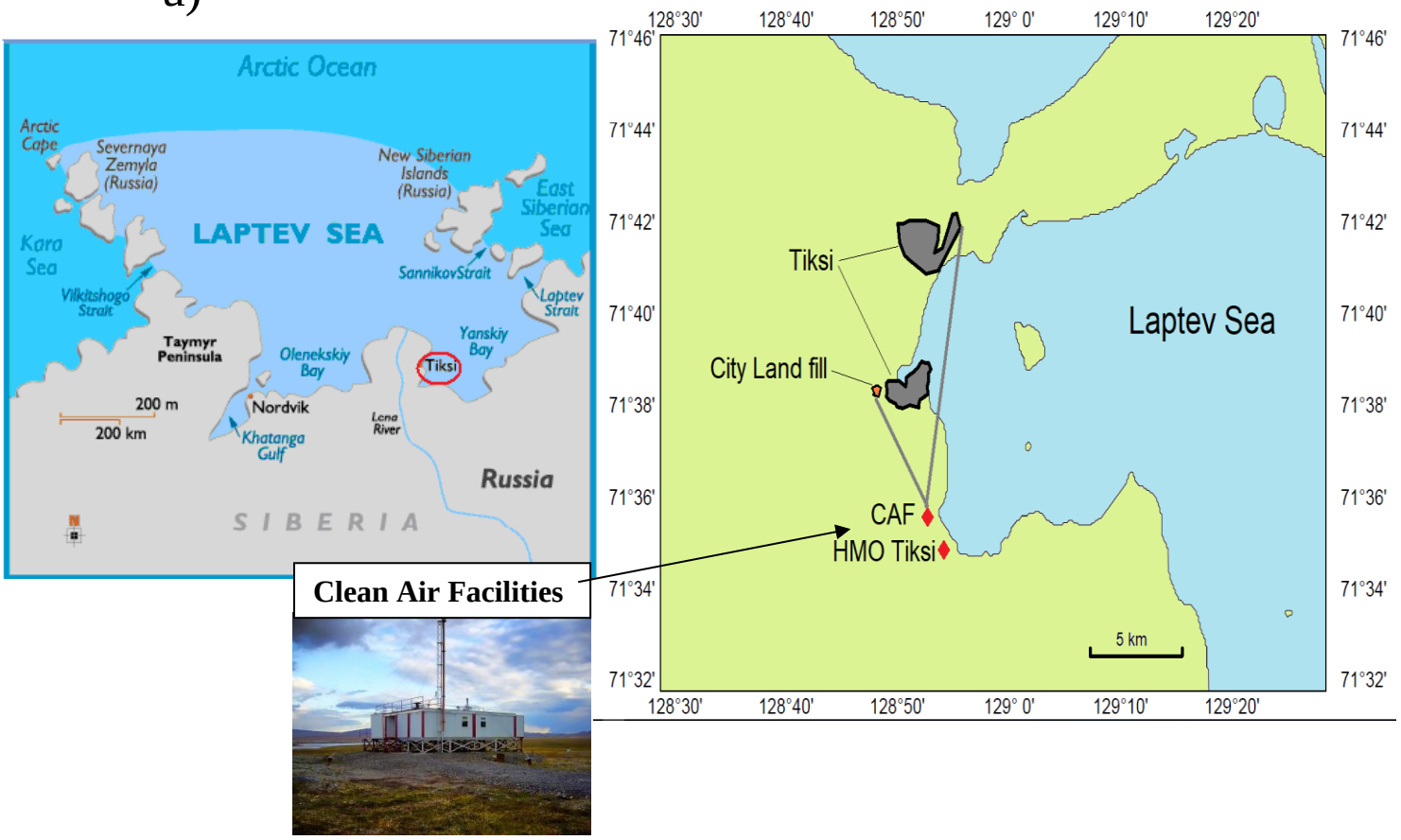

b)

Fig.1. a) Tiksi settlement in Northern Siberia; the area near Tiksi, an aerosol site Clean Air Facility (CAF) and HMO Tiksi (71.36N; 128.53E) is indicated and b) landfill burning plume at 15.09.2016, the photo was taken on the way from CAF to Tiksi. "Local Pollution Influence (LPI) sector" where from the local pollution affects the CAF is shown.

Table 1. Sampling periods at the CAF of HMO Tiksi; temperature *T*, pressure *p*, and *EBC* averaged over sampling period, OC/EC ratio.

period	time, hour	T,C^0	p, mbar	EBC, ng/m^3	OC/EC
Autumn 2014					
21.09-24.09	69	4	997	14	78
24.09-27.09	68.5	-0.6	1002	5	LOD
27.09-30.09*	69	-1.9	1004	18	-
30.09**	1.2	0.2	1011	97	-
30.09-01.10*	46	0.4	1013	125	-
Winter 2014					
20.11-22.11	48.6	-28	1001	141	10.87
22.11-24.11	44.3	-27	1019	179	8.97
24.11-26.11	45.9	-31	1008	237	2.83
26.11-27.11	20.3	-30	1013	146	6.1
Spring 2015					
19.03-20.03	22.5	-12,6	1000	150	18.44
20.03-21.03	22.5	-18	1000	220	15.17
21.03-22.03	23	-20	1009	158	22.35
Early summer 2015					
30.05-31.05	22.3	-1	1015	1.9	LOD
31.05-02.06	40.8	-0.4	1012	15.3	71.4
02.06-03.06	26.8	-1	1013	73.4	10.78
Autumn 2015					
06.09-08.09	47.3	11.2	1002	~	80.84
08.09-10.09	43	8.5	1011	40	42.16
Early summer 2016					
04.06-05.06	23.1	1.6	1012	50	86.5
05.06-07.06	45	4.1	1021	70	29.5
07.06-08.06	27.7	7.8	1018	100	50.8
Autumn 2016					
11.09-13.09	49.1	10.2	1026	61	80.9
13.09-15.09	43.2	7.7	1024	94	44.5

* Teflon filter, ** Ti foil. LOD- limit of detection.

Table 2. Aerosol techniques used.

Technique	Instrument	Type of substrates	Variables
Optical Attenuation	Magee Scientific Aethalometer	quartz	EBC
Thermo-optical Transmittance	Lab OC-EC Aerosol Analyzer	quartz	OC, EC
Capillary Electrophoresis	Capel 103 System (Lumex)	quartz	Water soluble inorganic anions (SO_4^{2-}, NO_3^-, Cl^-, F^-, PO_4^{3-}), cations (Na^+, NH_4^+, K^+, Mg^{2+}, Ca^{2+}), organic ions ($HCOO^-$, $CH3COO^-$, $(COO^-)_2$)
Fourier Transform Infrared Spectroscopy (FTIR)	Shimadzu IR Prestige-21 Spectrometer	quartz Ti foil	Organic and inorganic functionalities
X-Ray Florescence (XRF)	ED-XRF system	teflon	Elements Z=11-38 plus Ag, Cd, Sn, Sb, Cs, Ba, Ce, Pt, Au, Hg
Scanning Electron Microscopy, Energy Dispersive X-ray Spectroscopy (SEM/EDX)	LEO 1430-vp Zeiss system	Ti foil	Individual particles morphology and composition

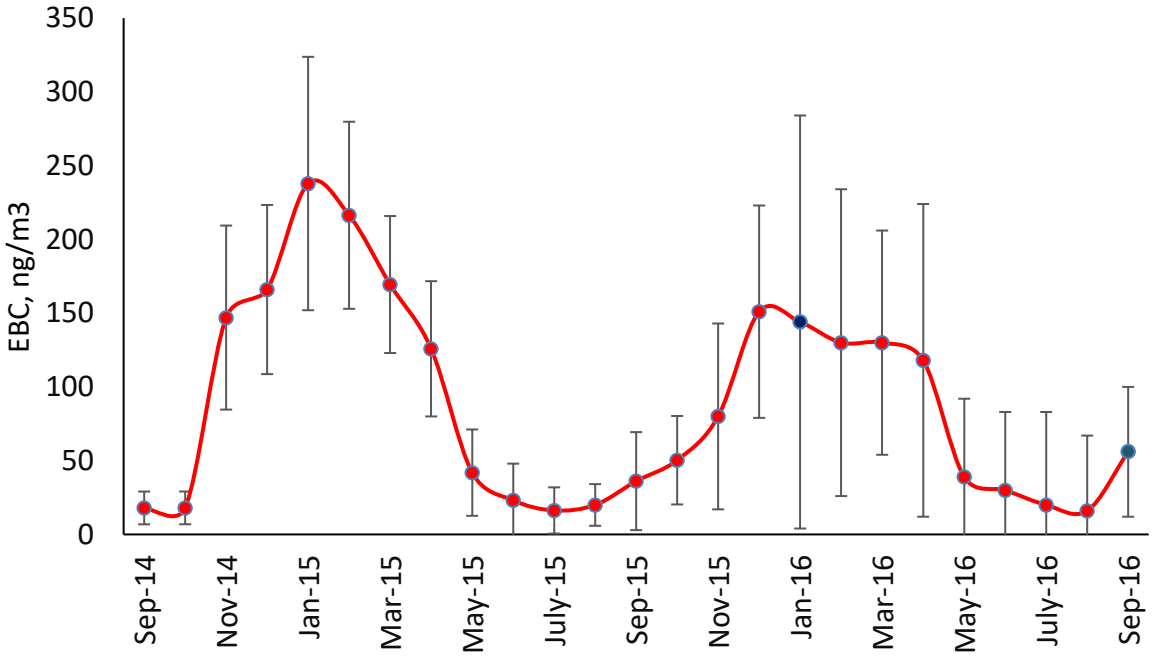

Fig.2. Monthly BC climatology from September 2014 to September 2016 at HMO Tiksi. Monthly means are presented by points with ± 1σ indicated by bars. Large σ value for January and September of 2016 (marked by blue) is decreased 3 times on the plot.

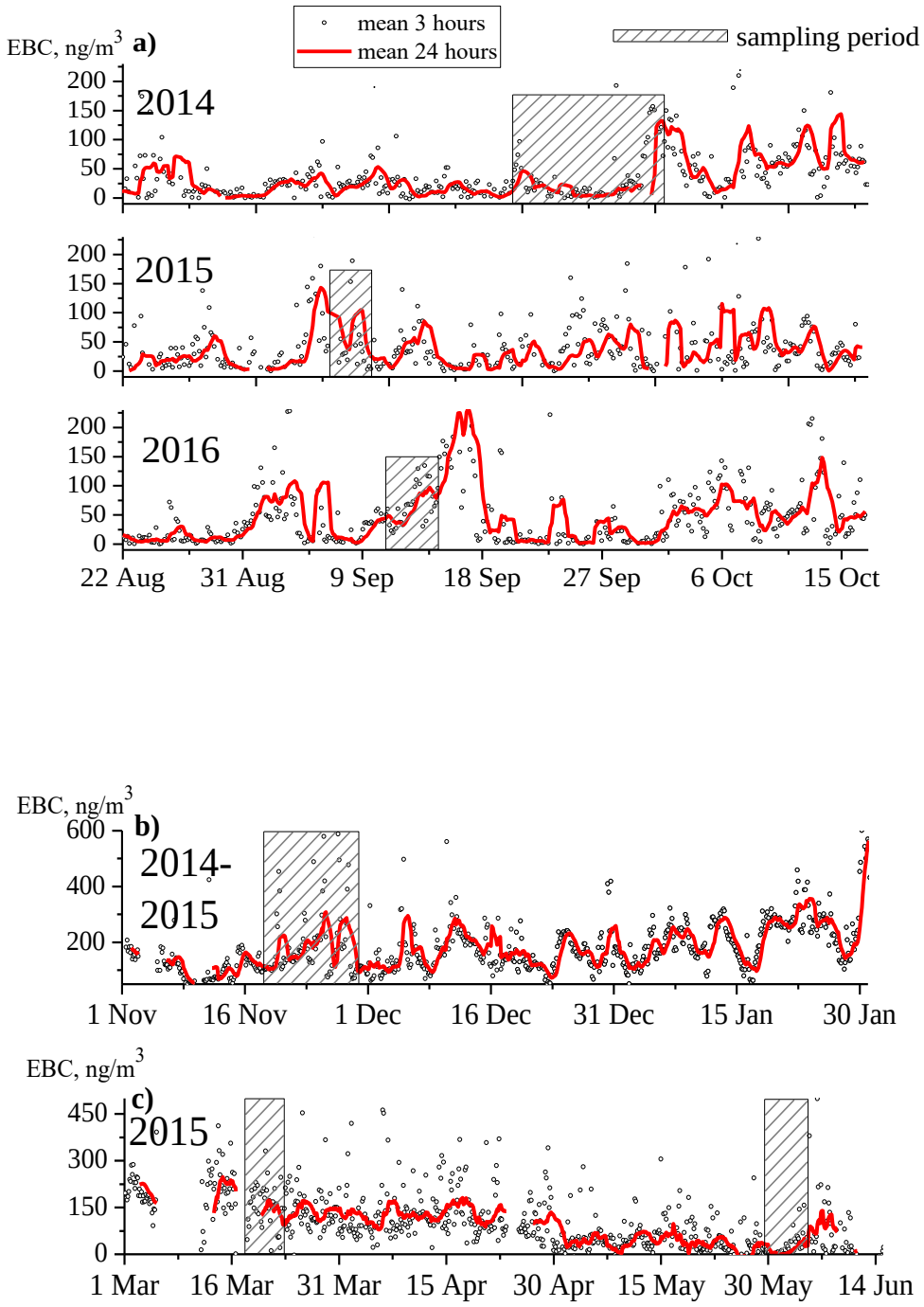

Fig.3. Time series of EBC concentrations from a) August to October of 2014, 2015, and 2016 year, b) November of 2014 to January 2015, and c) March to June 2015. 3 h means (points) and 24 h running means (curve). Episodes of sampling are marketed by square.

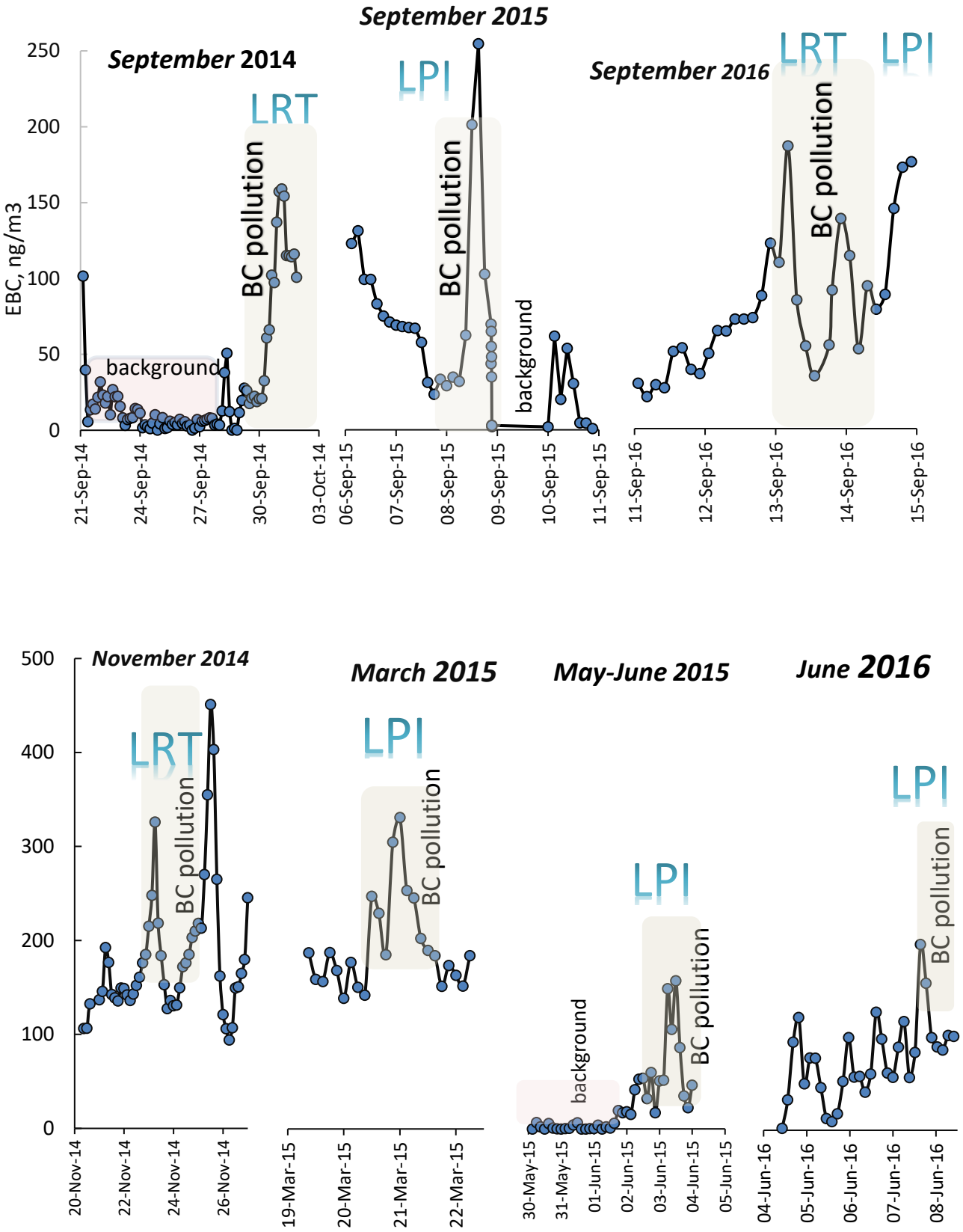

Fig. 4. EBC concentrations during sampling periods. Background is identified by lowest absorption. Episodes of the highest EBC pollution indicated as impacted by long-range air masses transportation (LRT) or local pollution influenced (LPI).

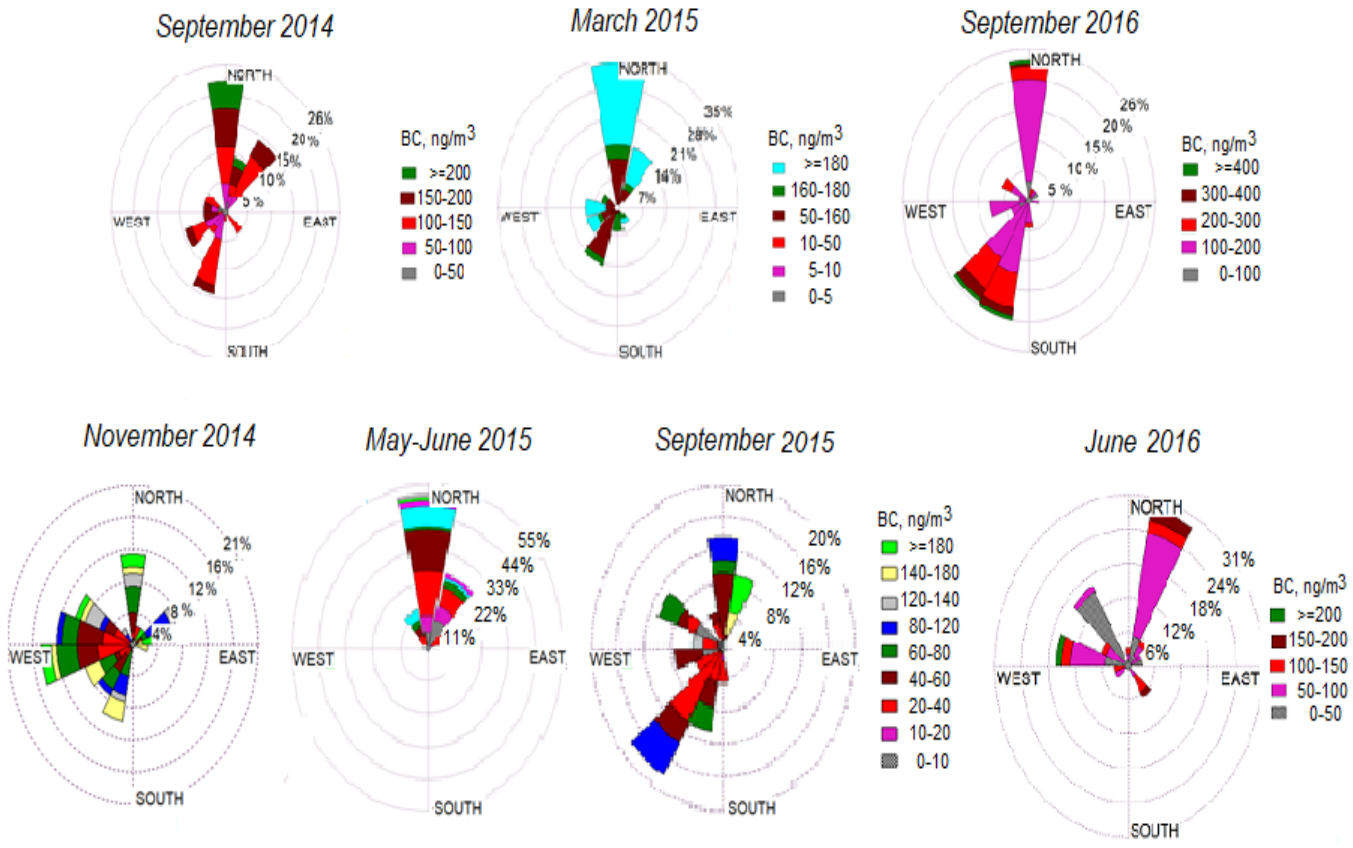

Fig. 5. Pollution rose of hourly averaged EBC concentrations during sampling periods of 2014, 2015 and 2016.

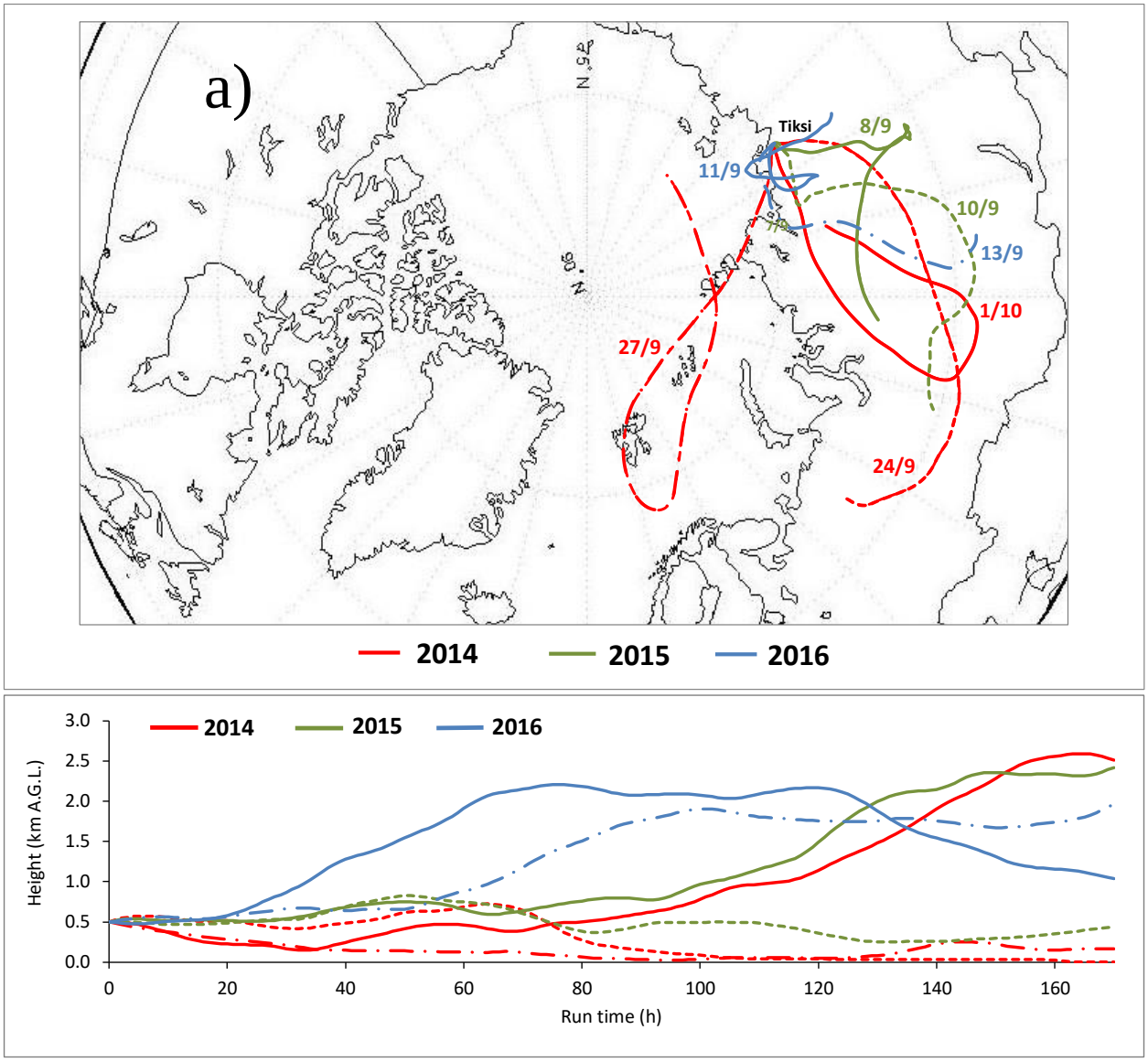
a)
Tiksi
8/9
11/9
10/9
13/9
1/10
27/9
24/9
2014
2015
2016
Height (km A.G.L.)
Run time (h)

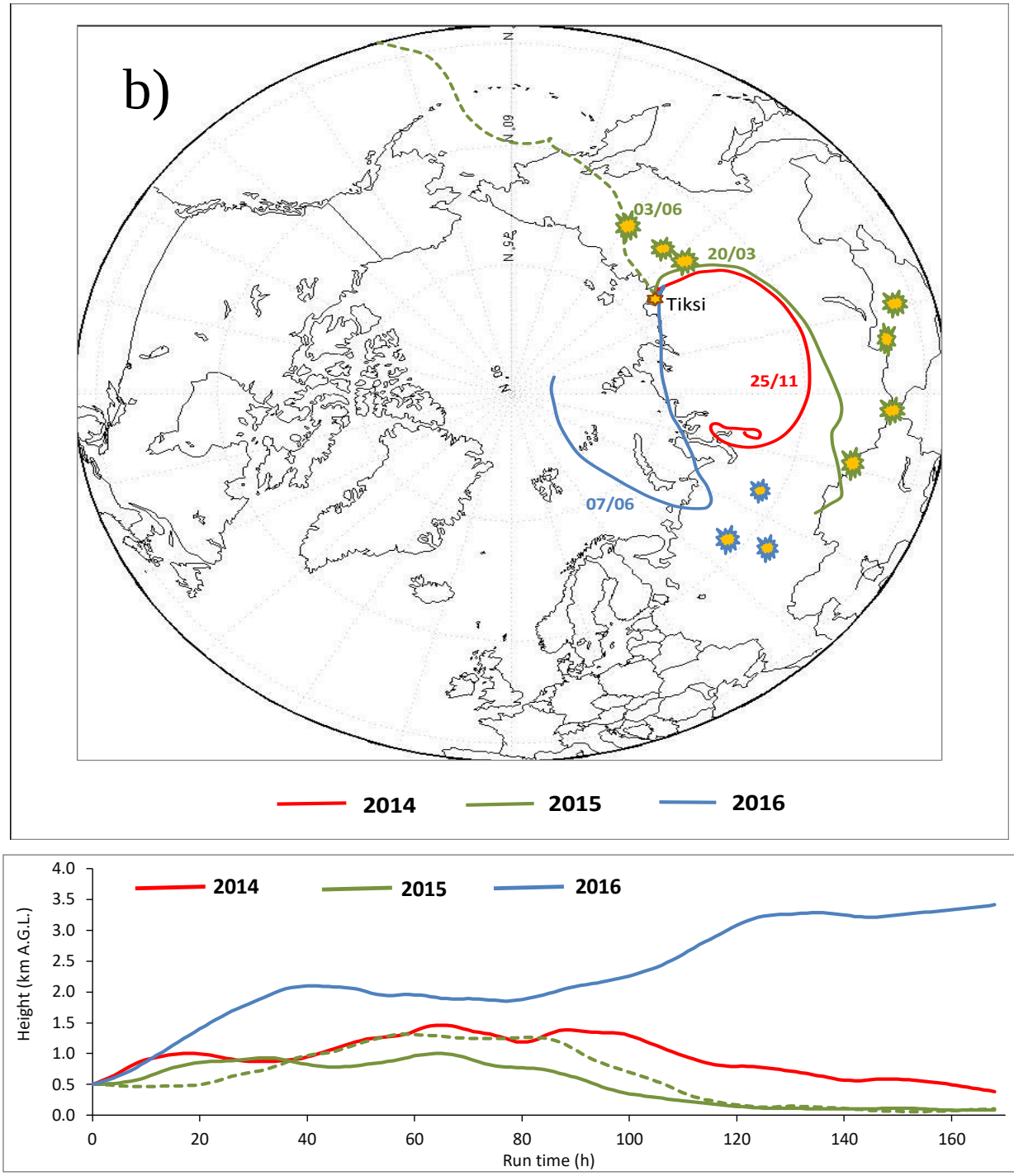

Fig. 6. 7-day air mass back trajectories arrived to HMO Tiksi in a case study in a) September 2014, 2015 and 2016, dashed and solid lines relate to background and EBC pollution episodes, and in b) November 2014, March 201, May-June 2015, and June 2016 for EBC pollution episodes. Trajectories generated for date indicated in 2014, 2015, and 2016 are marked in red, green, and blue color, respectively. Height A.G.L. of arrival is shown.

I suggest to make in red all what is concern to 2016 year (trajectory and fire spots) , and only for b).

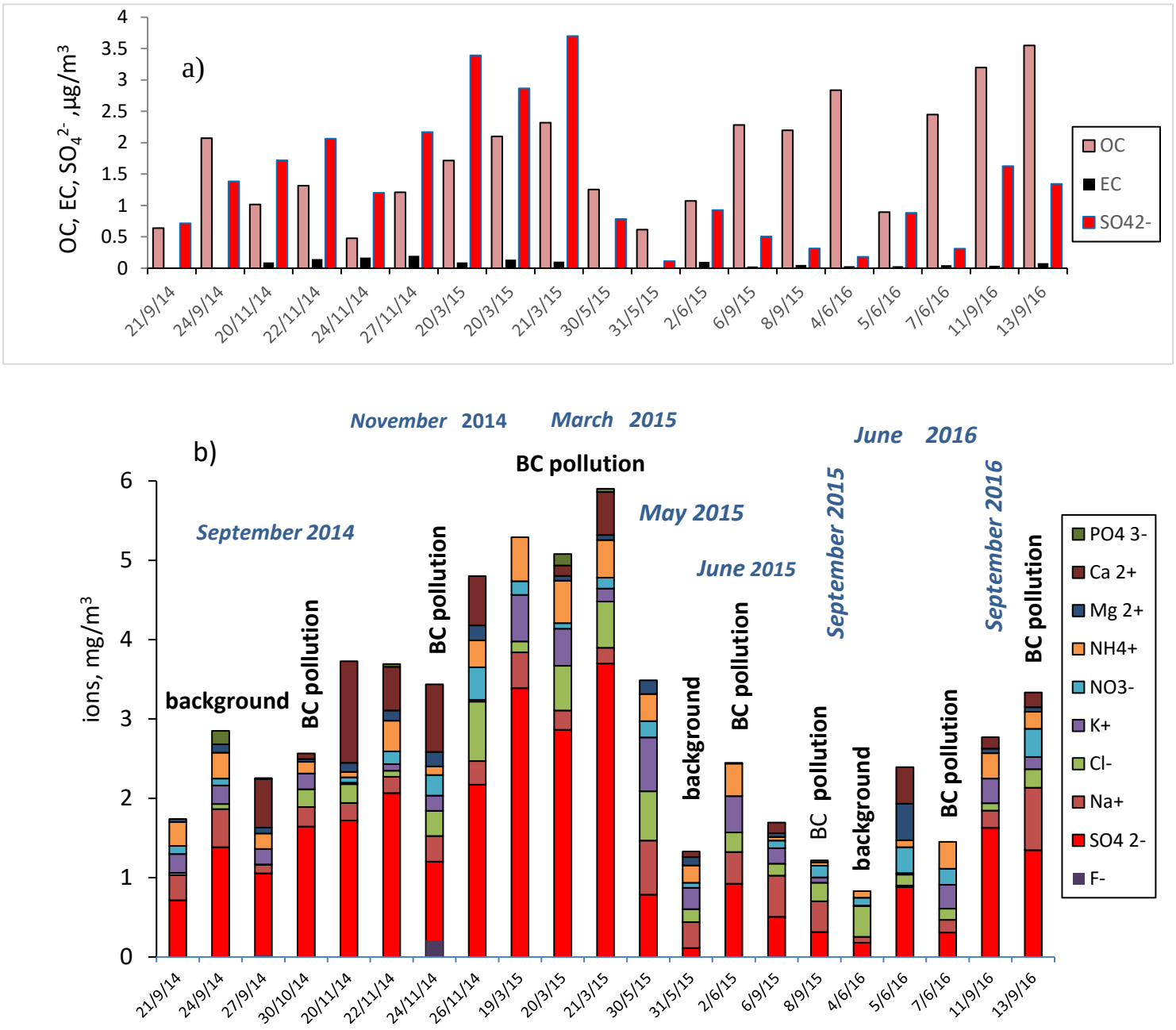

Fig.7.a) EC, OC, and SO_4^{2-}, and b) ion concentrations in sampling periods from September 2014 to September 2016.

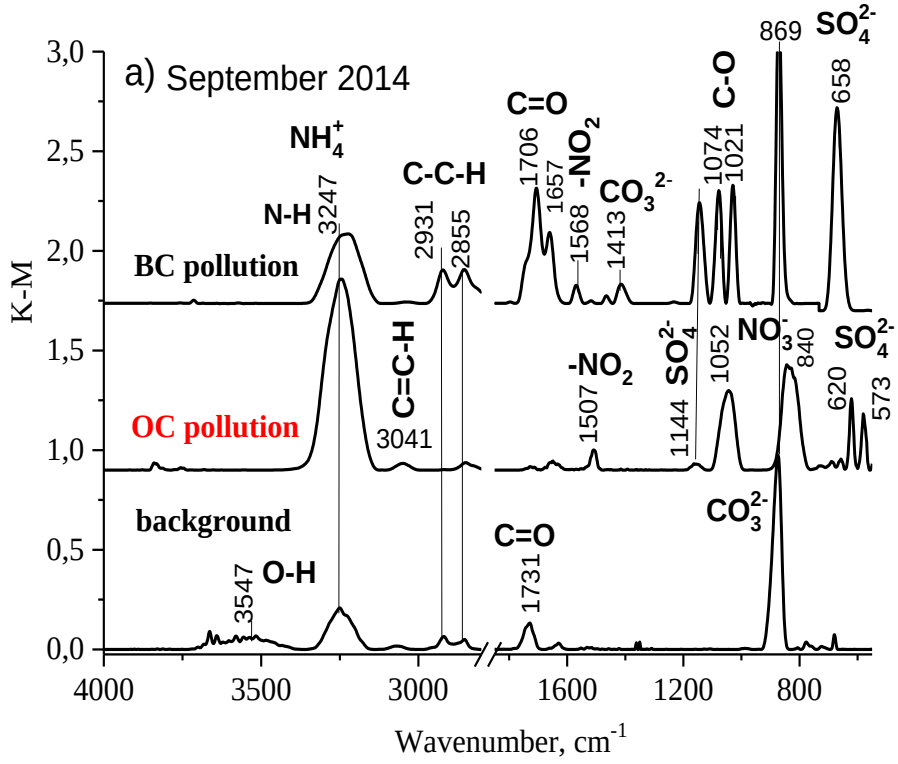
a) September 2014
K-M
3,0
2,5
2,0
1,5
1,0
0,5
0,0
BC pollution
OC pollution
background
N-H
3247
NH4+
C-C-H
2931
2855
C=O
1706
1657
-NO2
1568
CO3 2-
1413
C-O
1074
1021
869
SO4 2-
658
C=C-H
3041
-NO2
1507
SO4 2-
1144
1052
NO3-
840
SO4 2-
620
573
CO3 2-
O-H
3547
C=O
1731
4000
3500
3000
1600
1200
800
Wavenumber, cm-1

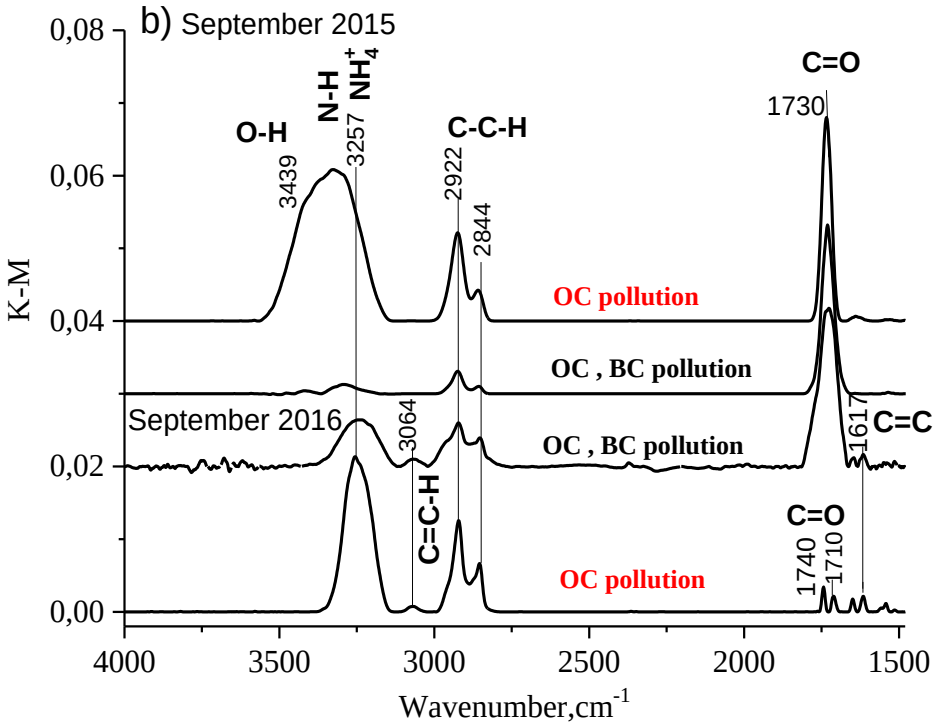
b) September 2015
K-M
0,08
0,06
0,04
0,02
0,00
O-H
3439
N-H
NH4+
3257
C-C-H
2922
2844
C=O
1730
OC pollution
OC , BC pollution
September 2016
3064
OC , BC pollution
C=C
1617
C=C-H
C=O
1740
1710
OC pollution
4000
3500
3000
2500
2000
1500
Wavenumber,cm-1

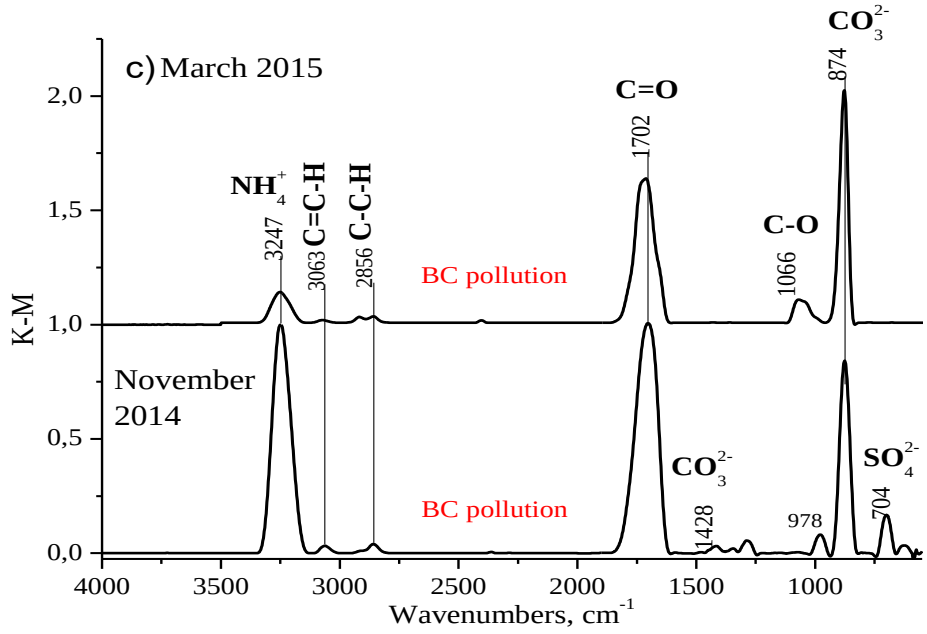
c) March 2015
K-M
2,0
1,5
1,0
0,5
0,0
NH_4^+
3247
C=C-H
3063
C-C-H
2856
BC pollution
C=O
1702
C-O
1066
CO_3^{2-}
874
November
2014
BC pollution
CO_3^{2-}
1428
978
SO_4^{2-}
704
4000
3500
3000
2500
2000
1500
1000
Wavenumbers, cm^{-1}

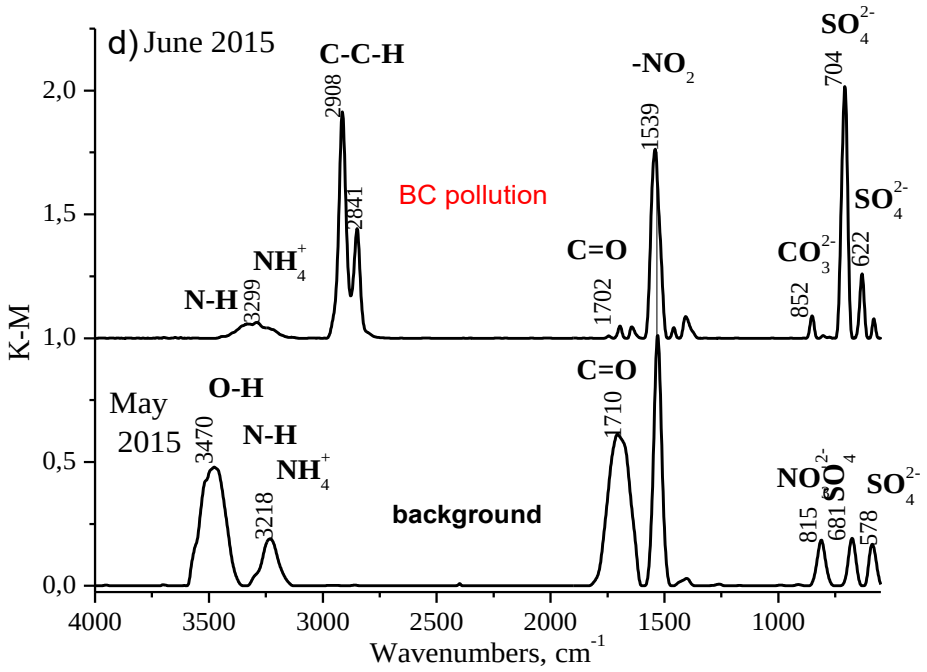
d) June 2015
K-M
2,0
1,5
1,0
0,5
0,0
C-C-H
2908
2841
$-NO_2$
1539
SO_4^{2-}
704
BC pollution
SO_4^{2-}
NH_4^+
N-H
3299
C=O
1702
CO_3^{2-}
852
622
May
2015
O-H
3470
N-H
NH_4^+
3218
C=O
1710
background
NO_3^{2-}
SO_4^{2-}
815
681
578
4000
3500
3000
2500
2000
1500
1000
Wavenumbers, cm^{-1}

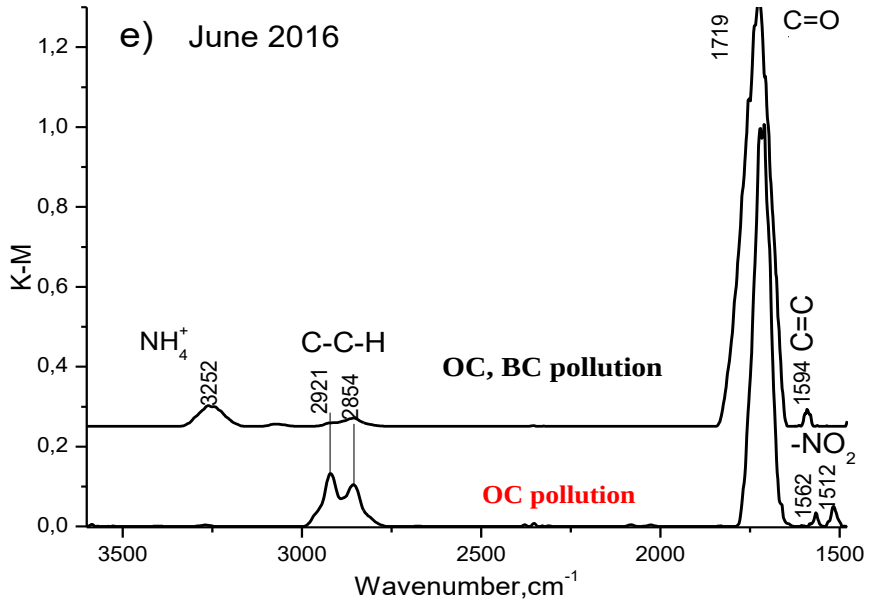

Fig.8. FTIR spectra of aerosols collected on days of background, OC and BC pollution in a) September 2014, and b) September 2015 and 2016, c) November 2014 and March 2015, d) May 2015 and June 2016, and e) June 2016. Absorption bands are indicated.

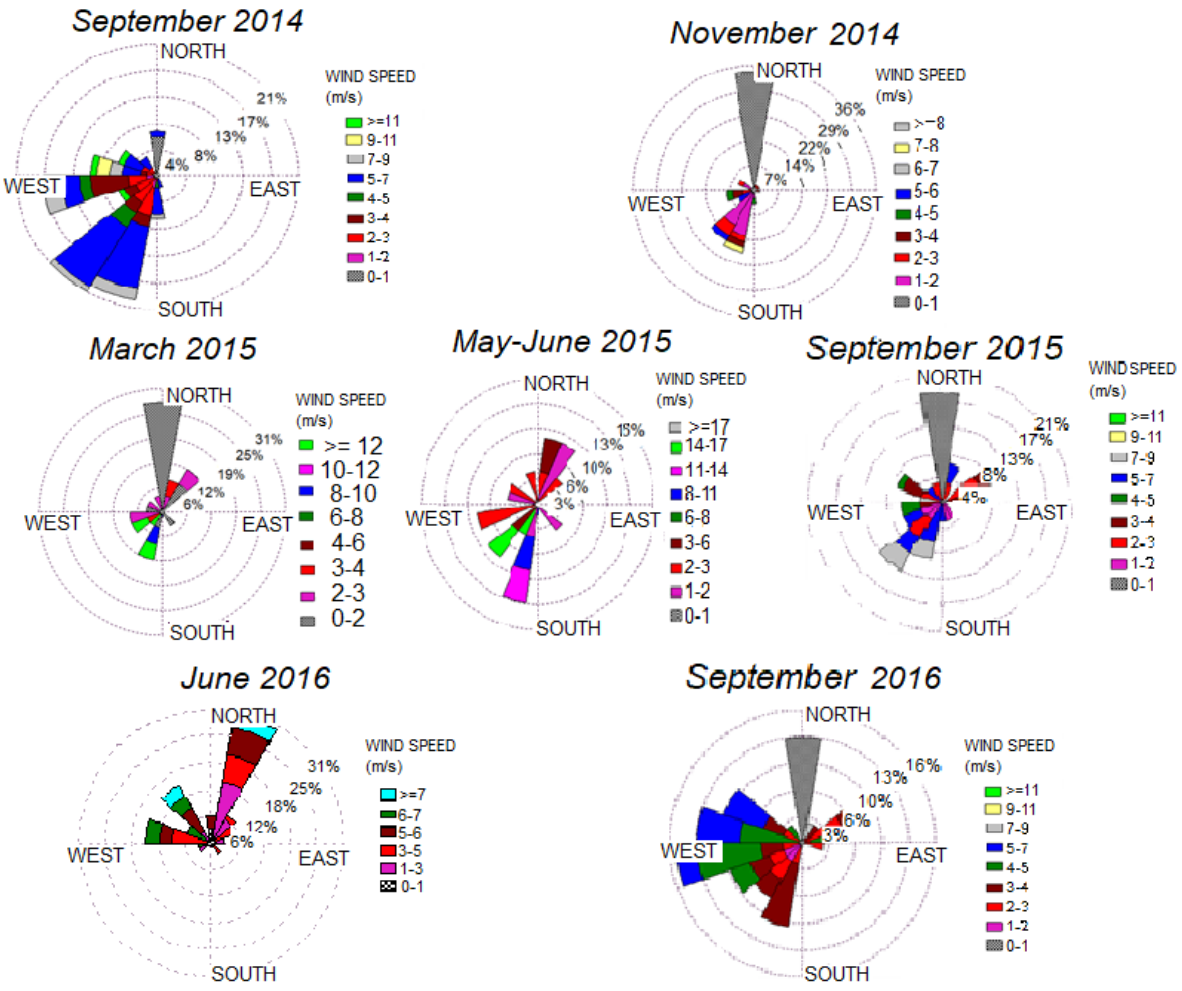

Fig.S1. Wind roses during the sampling periods from September 2014 to September 2016.

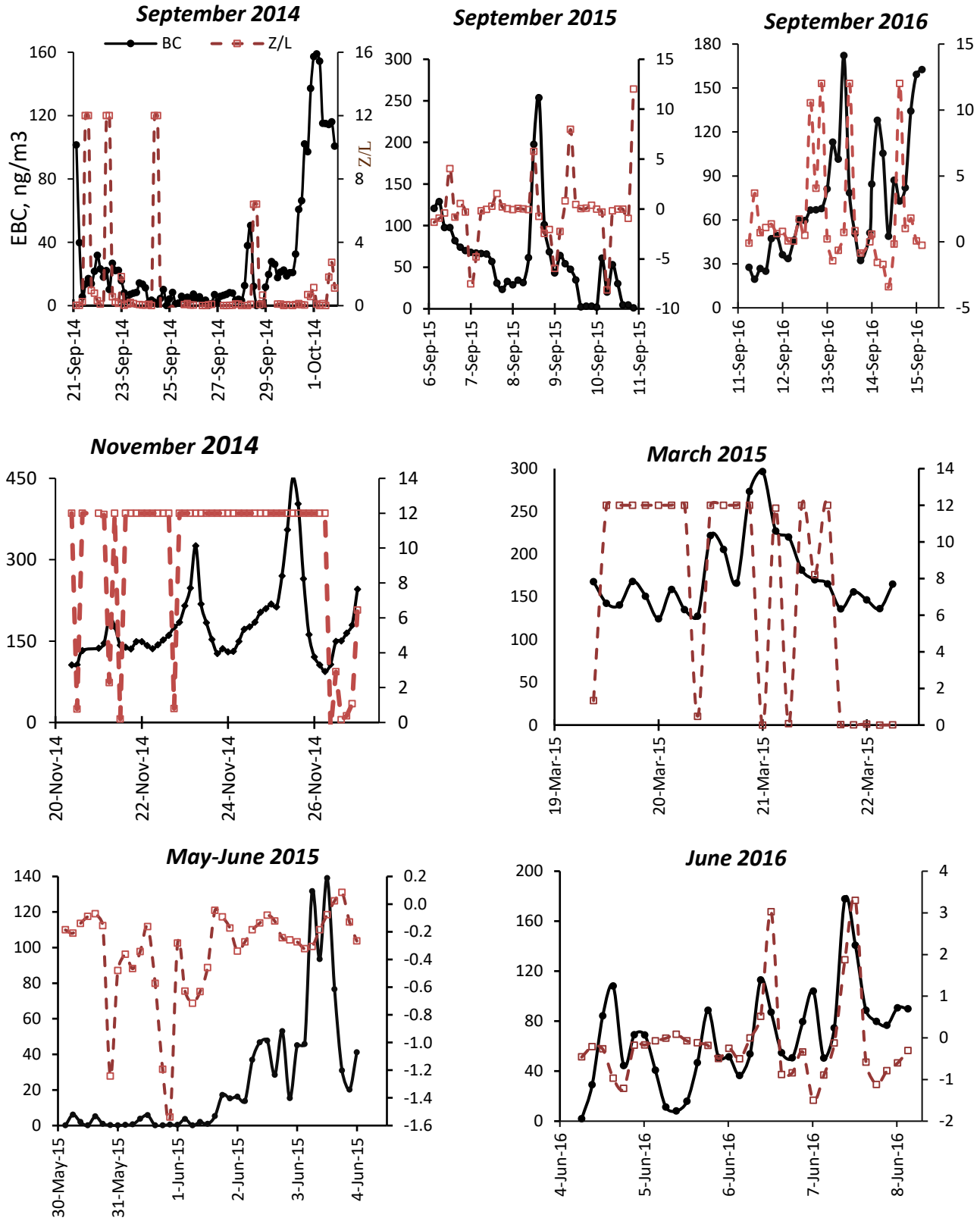

Fig.S2. EBC concentrations (left axis) and stratification parameter Z/L (right axis) during sampling periods.

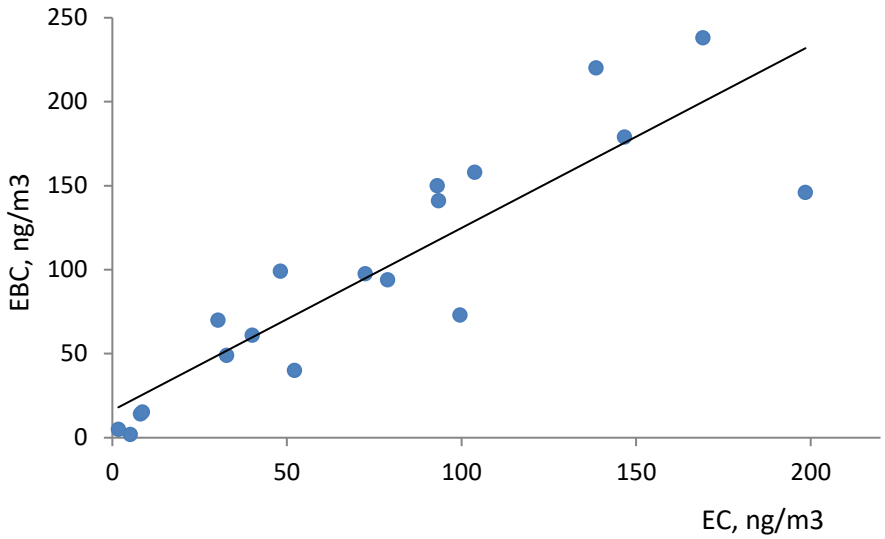

Fig.S3. Relationship between EBC concentrations averaged over the time of corresponding sample collection and EC concentrations during sampling periods from September 2016 to September 2016. The fitting line is obtained by linear regression with R^2=0.78 and slope=1.1.

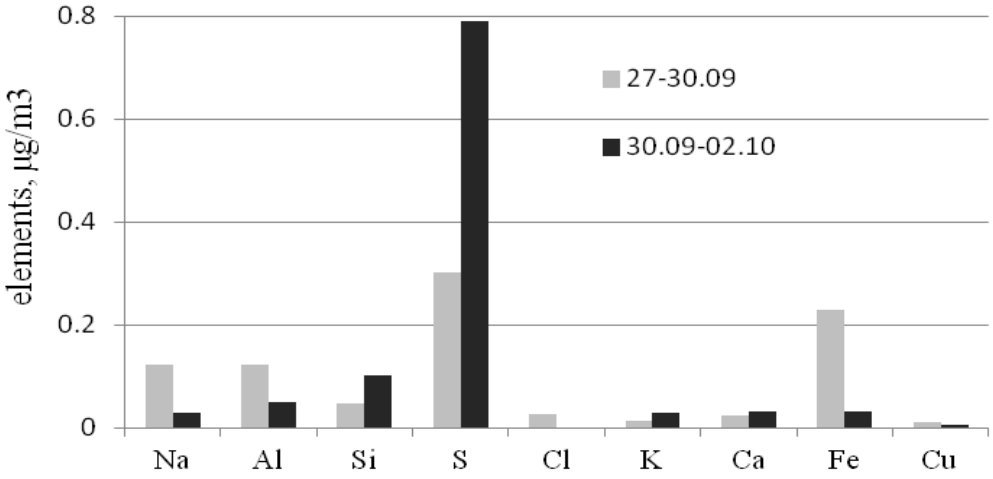

Fig.S4. Mass concentration of elements on 27-30.09 and during BC-pollution episode of 30.09-02.10.2014. Elements detected above 0.01 µg/m^3 are shown.